



# 1 **Acidification and nutrient management are projected to cause** 2 **reductions in shell and tissue weights of oysters in a coastal plain** 3 **estuary**

4 Catherine R. Czajka<sup>1</sup>, Marjorie A.M. Friedrichs<sup>1</sup>, Emily B. Rivest<sup>1</sup>, Pierre St-Laurent<sup>1</sup>, Mark J. Brush<sup>1</sup>,  
5 and Fei Da<sup>2</sup>

6 <sup>1</sup>Virginia Institute of Marine Science, William & Mary, Gloucester Point, VA, 23062, USA

7 <sup>2</sup>Department of Geosciences, Princeton University, Princeton, NJ, 08544, USA

8 *Correspondence to:* Catherine R. Czajka (czajkacatherine@gmail.com)

9 **Abstract.** Coastal acidification, warming, and nutrient management actions all alter water quality conditions that marine  
10 species experience, with potential impacts to their physiological processes. Decreases in calcite saturation state ( $\Omega_{Ca}$ ) and food  
11 availability, combined with warming water temperatures, pose a threat to calcifying organisms; however, the magnitude of  
12 future changes in estuarine systems is challenging to predict and is not well known. This study aims to determine how and  
13 where oysters will be affected by future acidification, warming, and nutrient reductions, and the relative effects of these  
14 stressors. To address these goals, an oyster bioenergetics model for Eastern oysters (*Crassostrea virginica*) was embedded in  
15 a 3-D coupled hydrodynamic-biogeochemistry model implemented for two tributaries in the lower Chesapeake Bay. Model  
16 simulations were forced with projected future conditions (mid-21st century atmospheric CO<sub>2</sub>, atmospheric temperature, and  
17 managed nutrient reductions) and compared with a realistic present-day reference run. Together, all three stressors are  
18 projected to reduce  $\Omega_{Ca}$  and growth of oyster shell and tissue. Increased atmospheric CO<sub>2</sub> and temperature are both projected  
19 to cause widespread reductions in  $\Omega_{Ca}$ . The resulting reductions in oyster shell and tissue growth will be most severe along the  
20 tributary shoals. Future warming during peak oyster growing seasons is projected to have the strongest negative influence on  
21 tissue and shell growth, due to summer water temperatures reducing filtration rates, enhancing shell dissolution and oyster  
22 respiration rates, and increasing organic matter remineralization rates, thus reducing food availability. Nutrient reductions will  
23 exacerbate deficits in oyster food availability, contributing to further reductions in growth. Quantifying the effects of these  
24 stressors provides insight on the areas in the lower bay where oysters will be most vulnerable to mid 21<sup>st</sup>-century conditions.

25  
26 **Short summary.** Under future acidification, warming, and nutrient management, substantial reductions in shell and tissue  
27 weights of Eastern oysters are projected for the Chesapeake Bay. Lower oyster growth rates will be largely driven by reduced  
28 calcium carbonate saturation states and reduced food availability. Oyster aquaculture practices in the region will likely be  
29 affected, with site selection becoming increasingly important as impacts will be highly spatially variable.



## 30 1 Introduction

31 Anthropogenic climate change and its associated impacts on water quality may threaten marine organisms and  
32 economic systems reliant on them. Oceanic uptake of increasing anthropogenic atmospheric carbon dioxide (CO<sub>2</sub>) causes a  
33 decrease in seawater pH and saturation states of calcium carbonate, a phenomenon known as ocean acidification (Caldeira and  
34 Wickett, 2003; Doney et al., 2009). Globally, the ocean has absorbed about 30% of anthropogenic atmospheric CO<sub>2</sub> since pre-  
35 industrial times (Gruber et al., 2019), and open-ocean surface pH is anticipated to decrease by 0.3 units on average relative to  
36 the 2010s by the end of the century under ‘business-as-usual’ conditions (Riahi et al., 2011; IPCC, 2019). The percent volume  
37 of ocean water undersaturated with calcite ( $\Omega_{Ca} < 1$ ) is predicted to expand to 91% by 2100 from 76% in the 1990s (Caldeira  
38 and Wickett, 2005; Gattuso et al., 2015).

39 Since estuaries have lower and more variable pH than the open-ocean, the effects of increased CO<sub>2</sub> on estuarine water  
40 quality and biota are often amplified. In coastal and estuarine systems, acidification may be exacerbated by local-level  
41 processes, such as the input of acidic freshwater and nutrient runoff from precipitation, a process termed coastal acidification  
42 (Salisbury et al., 2008; Wallace et al., 2014; Carstensen and Duarte, 2019). Freshwater has relatively low total alkalinity (TA),  
43 or buffering capacity, so areas in estuaries with greater relative freshwater influence cannot resist changes to pH as easily as  
44 more saline or open-ocean waters (Hasler et al., 2018; Pacella et al., 2024). Eutrophication, the increased rate of organic matter  
45 input to a system (Nixon, 1995), may drive large variations in local pH and overall water quality. Elevated nutrient inputs  
46 cause pH to increase in surface waters due to higher primary productivity, which will reduce surface acidification; however,  
47 pH will decrease in deeper bottom waters as the additional organic matter sinks and is remineralized (Cai et al., 2021).  
48 Management actions to reduce eutrophication and improve water quality in bottom waters have been successful but may also  
49 enhance acidification in shallow surface waters by lowering primary productivity (Borges and Gypens, 2010). The overall  
50 effect of future changes in nutrient inputs on coastal biogeochemistry is thus unclear.

51 Warming, another driver of biogeochemical change in coastal waters, may compound or offset the effects of increased  
52 atmospheric CO<sub>2</sub> on coastal ecosystems. The global ocean has absorbed approximately 93% of the atmospheric heat produced  
53 by anthropogenic activity, leading to a global sea surface temperature increase of 0.7°C since 1900 (Jewett and Romanou,  
54 2017). Ocean warming is expected to continue, with global averages increasing by 2.7°C by 2100 and greater increases  
55 expected in shallow coastal regions (Jewett and Romanou, 2017). Coastal acidification may accelerate as warming of coastal  
56 waters increases rates of biogeochemical processes; increased respiration rates may drive larger diel variations in pH, dissolved  
57 oxygen, and associated water quality (Du et al., 2018; Tian et al., 2021). Therefore, it is vital to understand how warming will  
58 interact with acidification to predict local changes in water quality and health of coastal organisms.

59 Characterizing spatiotemporal patterns of acidification in estuarine waters is important, as negative impacts of  
60 acidification on the biology of marine organisms may be substantial. Acidification disrupts the formation of calcium carbonate  
61 (CaCO<sub>3</sub>) during shell-building, i.e., biocalcification, which is a vital process for growth and survival of many aquatic  
62 invertebrate species (e.g., Orr et al., 2005; Gazeau et al., 2007; Dong et al., 2023). Under acidified conditions, water



63 concentrations of  $\text{CO}_2$  and  $\text{H}^+$  increase, and concentrations of carbonate ions ( $[\text{CO}_3^{2-}]$ ) decrease. A low ambient  $[\text{CO}_3^{2-}]$  inhibits  
64 calcifying organisms from forming  $\text{CaCO}_3$  for their shells, as more energy is required to precipitate  $\text{CO}_3^{2-}$  from acidified waters  
65 (e.g., Guinotte and Fabry, 2008; Lutier et al., 2022; Matoo et al., 2020; Mederios and Souza, 2023). Low  $\Omega_{\text{Ca}}$  may also lead to  
66 net dissolution of  $\text{CaCO}_3$ , leading to weaker shells and greater juvenile susceptibility to predation (e.g., Waldbusser et al.,  
67 2011; Amaral et al., 2012; Barclay et al., 2020). Acidification may further reduce shell growth through adverse physiological  
68 effects that limit energy availability for calcification. Because acidification is often more extreme in estuaries, oysters and  
69 other commercially valuable coastal bivalve species experience stronger effects of climate change than organisms living in  
70 open-ocean environments (Poach et al., 2019; Melzner et al., 2020; Cai et al., 2021; ). Prior experiments have revealed negative  
71 effects of acidification, warming, and nutrient reductions on oyster biocalcification and growth (Beniash et al., 2010;  
72 Waldbusser et al., 2011; Gobler and Talmage, 2014), but it is yet to be determined how the impacts of these stressors on oyster  
73 shell and tissue growth will vary spatially in highly dynamic systems.

74 The Chesapeake Bay is an excellent study system for examining the interacting influences of acidification, warming,  
75 and nutrient reductions (hereafter referred to collectively as “future stressors”) on estuarine biogeochemistry and the organisms  
76 living there. The bay exhibits high temporal and spatial variability in pH due to seasonal phytoplankton blooms, eutrophication,  
77 and acidic freshwater input (Da et al., 2021; St-Laurent et al., 2020; Kemp et al., 2005; Cai et al., 2021). From the mid-1980s  
78 to mid-2010s, surface waters in the upper bay experienced pH increases between +0.2 and +0.4 pH units in early spring and  
79 fall due to increased riverine TA from reduced acid mine drainage and lowered nitrate inputs, while surface waters in the  
80 nitrogen-limited middle bay decreased up to -0.24 pH units during late spring and summer as a result of decreased primary  
81 production (Da et al., 2021). Over the same time period, the bay warmed by  $0.24 \pm 0.15^\circ\text{C}$  per decade (Hinson et al., 2022),  
82 more than double the average rate of warming for the upper 75m of the global ocean (Rhein et al., 2013). Warming has also  
83 led to more severe hypoxia (Irby et al., 2018; Ni et al., 2020; Frankel et al., 2022; Hinson et al., 2023). In 2010, the  
84 Environmental Protection Agency mandated a Total Maximum Daily Load (TMDL) of pollutants from point and non-point  
85 sources to be achieved by 2025 (EPA, 2010). As nutrient reductions negatively affect pH in surface waters of the bay (Shen et  
86 al., 2020; Da et al., 2021), achieving the TMDLs may actually worsen acidification in shallow and near-shore regions. Much  
87 of the research effort devoted to characterizing present-day carbonate chemistry and its historical trends has focused on the  
88 mainstem and upper Chesapeake Bay (Cai et al., 2017; Shen et al., 2020, Su et al., 2020), and less is known about these  
89 conditions throughout the tributaries of the lower bay (Shadwick et al., 2019).

90 The combined effects of future stressors will impact calcifying organisms in the lower Chesapeake Bay as well as the  
91 economic systems reliant upon them. The Eastern oyster *Crassostrea virginica* (Gmelin, 1791) is a foundation species native  
92 to the bay (Dayton, 1972). Eastern oyster aquaculture in this region has grown rapidly in the past few decades, with Virginia  
93 becoming the third most productive oyster fishery in 2018 (Hudson, 2019), largely a result of the development of disease-  
94 resistant oyster strains (Frank-Lawale et al., 2014). Negative impacts of acidification on aquaculture practices in other parts of  
95 the world (Barton et al., 2015) have already stirred concern over the vulnerability of oysters in the Chesapeake Bay. For  
96 example, in the Pacific Northwest, major larval mortality occurred at a shellfish hatchery following an upwelling event that



97 lowered pH and  $\Omega$  of aragonite, which had cascading impacts on the oyster industry all along the West Coast (Barton et al.,  
98 2015). While most effects of acidification on aquaculture have been observed in oyster larvae in hatcheries, fewer studies have  
99 examined acidification's influence on adult oysters when deployed in the field. Water quality conditions within oyster farms  
100 can be highly spatially variable, so the impacts of acidification may vary with growing conditions (Saavedra et al., 2024;  
101 Simpson et al., 2024). To support the future of the oyster aquaculture industry in Chesapeake Bay, it is critical to identify  
102 which areas in the bay will be most vulnerable to acidification at mid-century and how each driver of change contributes to  
103 acidification and its impacts on growth.

104 This study addresses the following primary research question: How and where will carbonate chemistry and Eastern  
105 oyster growth in the lower Chesapeake Bay change in the future and which future stressors will drive these changes? A three-  
106 dimensional hydrodynamic-biogeochemical model is coupled with an oyster bioenergetics model and is applied to two major  
107 Virginia tributaries of the Chesapeake Bay. The model provides detailed information on present-day environmental conditions,  
108 and when combined with climate projections from Earth System Models, allows for simulations of the independent and  
109 interacting influences of future environmental change on carbonate chemistry and Eastern oysters. This study provides insight  
110 into which areas are most vulnerable to mid 21<sup>st</sup>-century acidification and how acidification, warming, and nutrient loading  
111 may each impact oyster growth in isolation as well as via simultaneous co-stressors.

## 112 **2 Methods**

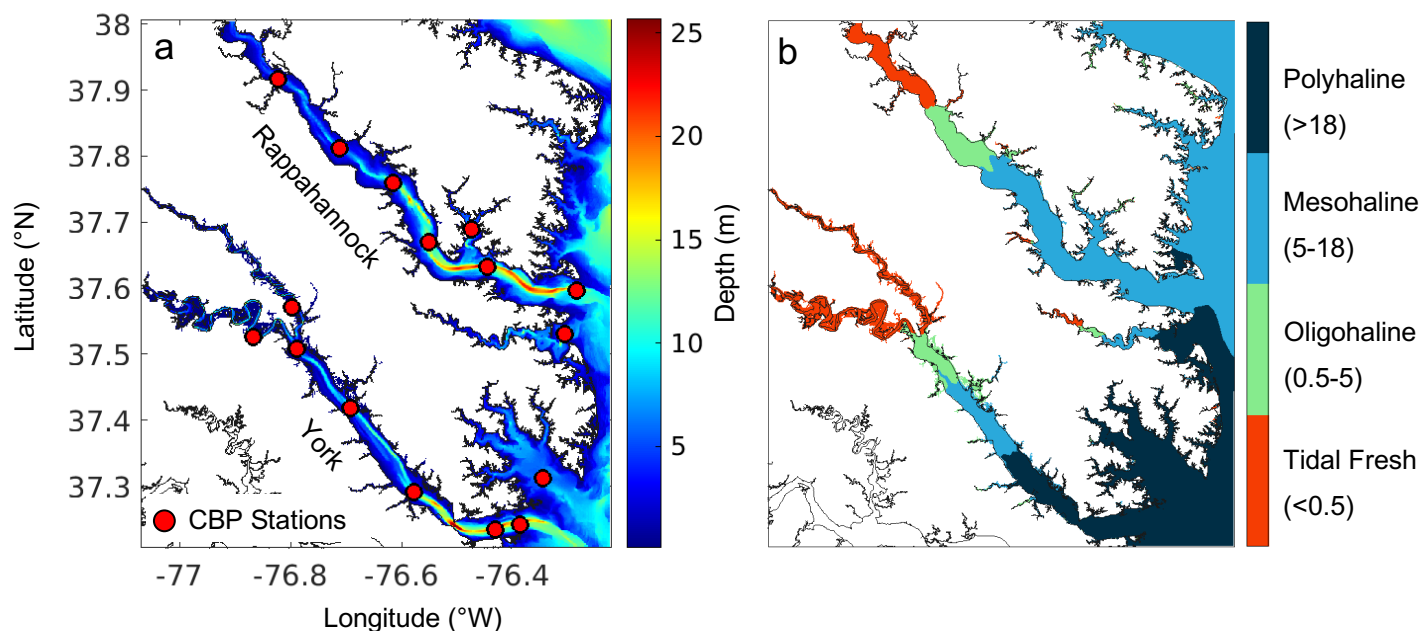
### 113 **2.1 Model description**

#### 114 **2.1.1 Hydrodynamic model**

115 This study uses the three-dimensional hydrodynamic Regional Ocean Modeling System (ROMS; Shchepetkin and  
116 McWilliams, 2005), implemented similarly to St-Laurent and Friedrichs (2024) but on a higher resolution grid focused on two  
117 of the lower Virginia Chesapeake Bay tributaries (Fig. 1). The model domain (Da et al., 2024) includes the York and  
118 Rappahannock Rivers, as well as a portion of the mainstem shoal north of the Rappahannock. The model grid consists of  
119 620x740 horizontal grid cells with a horizontal resolution of 120 m, allowing for greater resolution of coastlines than many  
120 other Chesapeake Bay model grids (Irby et al., 2016). The hydrodynamic model includes 20 terrain-following vertical levels  
121 and two primary state variables: practical salinity and potential temperature. A wetting and drying scheme has been  
122 implemented to represent water levels and currents in coastal grid cells (Warner et al., 2013; St-Laurent and Friedrichs, 2024).



123



124 **Figure 1. ROMS-ECBO model domain of Chesapeake Bay tributaries illustrating (a) bathymetry in meters and locations of**  
125 **Chesapeake Bay Program (CBP) water quality monitoring stations (red circles) and (b) bottom salinity zones.**

## 126 2.1.2 Carbon and biogeochemistry model

127 The Estuarine-Carbon-Biogeochemistry model (ECB) embedded in ROMS and used in this study has previously been  
128 implemented in the Chesapeake Bay (Feng et al., 2015; St-Laurent et al., 2020; Frankel et al., 2022; Hinson et al., 2023) as  
129 well as in the lower Virginia tributaries (Da et al., 2024). ECB simulates full carbon and nitrogen cycles of the lower trophic  
130 levels, represented by the following state variables: nitrate, ammonium, phytoplankton and zooplankton nitrogen, small and  
131 large detrital nitrogen and carbon, semi-labile and refractory dissolved organic nitrogen, DIC, TA, and dissolved oxygen (O<sub>2</sub>).  
132 Phytoplankton and zooplankton carbon and dissolved organic carbon (DOC) are calculated from established C:N ratios  
133 (Redfield, 1934; Hopkinson et al., 1998). Biogeochemical processes include primary production, aggregation, sinking, basal  
134 metabolism, exudation, sloppy feeding, excretion, metabolism, nitrification/denitrification, remineralization, grazing, and  
135 mortality. Additional biogeochemical sources and sinks are included in the bottom vertical level (e.g., burial, resuspension,  
136 nitrification/denitrification, remineralization, sediment O<sub>2</sub> and CO<sub>2</sub> exchange). Light attenuation throughout the water column  
137 is based on the diffuse attenuation coefficient (K<sub>d</sub>), which is parameterized as a function of surface total suspended solids  
138 (TSS; including inorganic and organic components) and salinity as a proxy for colored dissolved organic matter (Feng et al.,  
139 2015; Turner et al., 2021). The sediment transport module within ECB is comprised of two vertical seabed layers that simulate  
140 four suspended sediment size classes (Turner et al., 2021).



141 The carbon module within ECB has been fine-tuned in this implementation of the model, allowing for greater  
142 performance in carbonate system simulations (Da et al., 2024). The model grid includes tidal wetlands along the York River  
143 based on estimated wetland areas (Mitchell et al., 2017), which further contribute to TA fluxes through sulfate reduction in  
144 sediments (Raymond et al., 2000; Najjar et al., 2020).  $\Omega_{Ca}$  is calculated from DIC, TA, temperature, and salinity using CO2SYS  
145 (van Heuven et al., 2011) using the equilibrium constants of Cai and Wang (1998) as they are suitable for both fresh and  
146 estuarine waters (Dinauer and Mucci, 2017; Herrmann et al., 2020). Although submerged aquatic vegetation is a possible  
147 source of  $CaCO_3$  (Mazarrasa et al., 2015; Su et al., 2020),  $CaCO_3$  precipitation and dissolution are not simulated in ECB due  
148 to both insufficient observations and low submerged aquatic vegetation presence throughout the model domain (Orth et al.,  
149 1998; Moore et al., 2009).

150 Several updates have been made in this implementation of ROMS-ECB to better represent oxygen and primary  
151 production dynamics in the lower Virginia tributaries. The minimum phytoplankton growth rate has been increased to  $2.15 \text{ d}^{-1}$ ,  
152 and the growth rate is limited in the fresh portion of the tributaries using a Michaelis-Menten function of salinity and a half-  
153 saturation of 1.5 (Da et al., 2024). The sediment bed climatology from Moriarty et al. (2021) has been adjusted to better  
154 represent the sand class distributions published in Nichols (1991) and observations taken by the USGS (Reid et al., 2005).  
155 Specifically, the changes include a greater percentage of small clay-rich flocs throughout the main stem of the York River as  
156 well as more sand and large silt-rich flocs in the Rappahannock River. Previously, the sediment module assumed the same  
157 critical shear stress for large silt-rich flocs, small clay-rich flocs, and unaggregated mud; here, the critical shear stress of smaller  
158 particles is lower than larger particles, meaning smaller particles resuspend more easily. The updated critical shear stress  
159 coefficient for erosion and deposition is 0.5 Pa for large silt-rich flocs and 0.4 Pa for both small clay-rich flocs and  
160 unaggregated mud, which represent a small portion of the sediment bed. The ballasting formulation of Turner et al. (2021) has  
161 also been added to simulate the increase in particle sinking rates due to the aggregation of particles in turbid waters.

### 162 **2.1.3 Oyster bioenergetics model**

163 As part of this study, the oyster bioenergetics model EcoOyster (Brush and Kellogg, 2018; Kellogg et al., 2018) has  
164 been one-way coupled to ROMS-ECB in the deepest (bottom) level (see Supplementary Tables S1-S4 for EcoOyster  
165 equations). The one-way coupling allows the focus in this analysis to be on the effect of future climate change on oyster  
166 growth, rather than the effect of oyster growth on water quality, which has been previously studied in the Chesapeake Bay  
167 (e.g., Gawde et al., 2024). By focusing on the deepest vertical level of the model, the assumption is that oysters are growing  
168 on the bottom, and not inside floating cages. The coupled model, referred to hereafter as ROMS-ECBO, simulates daily somatic  
169 tissue dry weight, gonadal tissue dry weight, shell dry weight, and shell height of diploid and triploid oysters as a function of  
170 filtration, respiration, egestion, allocation to reproduction, calcification, and dissolution (Brush and Kellogg, 2018; Kellogg et  
171 al., 2018; Rivest et al., 2023). For the purpose of this study, only diploid oysters were included, as the triploid allometric  
172 equations are not as well constrained. Tissue growth rates depend on individual weight together with temperature, salinity,  $O_2$ ,  
173 TSS, and particulate organic carbon (POC) from ROMS-ECB.  $Chla$  is required for the filtration function and is calculated



174 from ROMS-ECB phytoplankton carbon and  $K_d$ , in combination with seasonal carbon:chl $a$  ratios that are computed using  
175 equations from Cerco and Noel (2004). The calcification function includes a threshold value of  $\Omega_{Ca} = 0.93$ , determined through  
176 laboratory experiments with Eastern oysters (Rivest et al., 2023).

177 The *EcoOyster* equations were developed from a meta-analysis of existing oyster bioenergetics models and laboratory  
178 experiments with diploid oysters (Brush and Kellogg, 2018; Kellogg et al., 2018; Rivest et al., 2023). Allometric relationships  
179 between shell dry weight, tissue dry weight, and shell height used for initial conditions were derived from observational data  
180 in the Chesapeake Bay (VOSARA, 2024). Total dry tissue weight is calculated as the sum of somatic tissue weight and gonadal  
181 weight. Reproduction is simulated through gonadal weight, a function of growth of gonadal tissue, resorption of gonadal tissue,  
182 and spawning (Hofmann et al., 1994). Somatic tissue weight is a function of assimilation, respiration, growth of gonadal tissue,  
183 and resorption of gonadal tissue. Assimilation is a function of filtration and POC. Filtration is a function of a maximum  
184 filtration rate based on tissue weight, limited by sub-optimal temperature, salinity, TSS,  $O_2$ , and chl $a$  (Cerco and Noel, 2005;  
185 Fulford et al., 2007; Ehrich and Harris, 2015). The optimal temperature for oyster filtration ( $T_{opt}$ ) is set to 27 °C (Jordan, 1987).  
186 Filtration is also multiplied by  $p$ , a tunable factor representing the proportion of computed filtration actually performed by  
187 oysters, which accounts for processes excluded from the model such as time spent filtering and is constrained by published  
188 growth rates. Respiration is a function of tissue weight, temperature, and assimilation. While filtration has a temperature  
189 limitation, respiration increases exponentially with temperature (Fig. S1). Tissue growth functions are not affected by  
190 carbonate chemistry variables, as experimental studies have found that neither filtration (Lemasson et al., 2018) nor respiration  
191 (Beniash et al., 2010; Matoo et al., 2013) of oysters are affected by pH changes; however, weight-specific net calcification is  
192 a function of  $\Omega_{Ca}$  and temperature (Rivest et al., 2023). Shell growth is a function of both total tissue weight and net  
193 calcification.

## 194 2.2 Present day reference simulation

195 A realistic reference simulation was generated to represent 2017 conditions. The year 2017 was chosen for  
196 atmospheric, terrestrial, and open-ocean boundary conditions as this represents a relatively typical hydrological year.  
197 Atmospheric forcings (air temperature, long- and short-wave radiation, precipitation, winds, dewpoint temperature, and air  
198 pressure) are obtained from the ERA5 atmospheric reanalysis (Copernicus Climate Change Service, 2017; Hersbach et al.,  
199 2020). Surface atmospheric variables are available at 3-hourly intervals with a 0.25° resolution and are interpolated to a 0.2°  
200 grid. Terrestrial inputs of freshwater, nitrogen, carbon, and sediment are derived from the Phase 6 CBP Watershed Model  
201 (CBPWM; Bhatt et al., 2023) and USGS data. Daily estimates of freshwater discharge, water temperature, and loadings of  
202 nitrate, ammonium, organic nitrogen, and four classes of sediment from the CBPWM were concatenated to 74 locations  
203 throughout the model domain. To compute carbon loadings, constant carbon-to-nitrogen ratios are used, specifically 10:1 for  
204 dissolved organic matter (Hopkinson et al., 1998) and 6.625:1 for particulate organic matter (Redfield, 1934). Riverine TA  
205 concentrations are computed as in Da (2023), using monthly-varying linear relationships between historical USGS  
206 observations of discharge and USGS TA estimates determined using the Weighted Regression on Time, Discharge, and Season



207 (WRTDS; Hirsch et al., 2010) approach. Riverine DIC is calculated from daily riverine TA and daily DIC:TA ratios, linearly  
208 interpolated from the monthly climatology of USGS WRTDS DIC:TA in each tributary. As in Da (2023), open boundary  
209 conditions are derived from a recent 600 m resolution whole-bay implementation of ROMS (St-Laurent and Friedrichs, 2024).  
210 Initial conditions for the six-month spin-up were derived from previous model results (Da et al., 2024).

211 Since spring-spawned oysters are typically deployed in late spring through summer on oyster farms, the reference run  
212 was started on July 1<sup>st</sup> and spanned one full year, ending June 30<sup>th</sup> of the following year. Oyster sizes were initialized based  
213 on shell height approximations of a typical spring-spawned oyster at deployment in July (i.e., a few months old). Starting dry  
214 tissue weight was assumed to be 0.001 g for all oysters, back-calculated from the approximate height of an oyster at the time  
215 of deployment. Starting shell dry weights and heights were calculated from allometric relationships to be 0.144 g and 11.6  
216 mm, respectively.

### 217 **2.3 Comparison of reference simulation to in situ observations**

218 *In situ* water quality monitoring observations are available since 1984 throughout the Chesapeake Bay. Specifically,  
219 the Chesapeake Bay Program's Water Quality Monitoring Program (CBP WQMP) conducts cruises in the Bay and its  
220 tributaries. On average, stations are sampled once monthly, with the exception of June through August in the mainstem, when  
221 sampling occurs twice. In this study, measurements of water temperature, salinity, O<sub>2</sub>, pH (NBS scale), TSS, and POC are  
222 used from 16 CBP stations throughout the model domain, with depths ranging from 5 to 16 m (Fig. 1a; CBP, 2024). For all  
223 variables except TSS and POC, measurements are taken *in situ* using a YSI or Hydrolab® sonde roughly every one to two  
224 meters of the water column. TSS and POC are obtained from bottle samples at the surface, bottom, and at deeper stations, two  
225 additional depths above and below the pycnocline. TSS is determined by filtering a known volume of water through a pre-  
226 weighted filter and then re-weighing the filter after filtration and drying. POC is determined through combustion of a filter  
227 using an elemental analyzer (Olsen, 2012).

228 Model skill was evaluated by comparing results from the reference simulation to the CBP WQMP observations  
229 described above. Hourly outputs from the four closest grid cells to each CBP station were spatially interpolated to obtain results  
230 at each respective station. Multiple variables in ECB at the bottom level of the model, including temperature, salinity, O<sub>2</sub>, pH,  
231 TSS, and POC, were compared with observations from the same station and time, within the bottom 10% of the water column  
232 (Table 1). Model bias and root-mean squared difference (RMSD) were computed for all aforementioned variables. Seasonal  
233 skill was also evaluated by comparing the 2017 reference run to CBP decadal averages (Figs. 2, 3). Decadal means were used  
234 for these comparisons, as once-monthly or once-seasonally sampling dates in 2017 bias outputs toward conditions on the time  
235 of the month when the measurements were taken in 2017, and the purpose of the comparison was to examine how the model  
236 reproduces average seasonal variability.

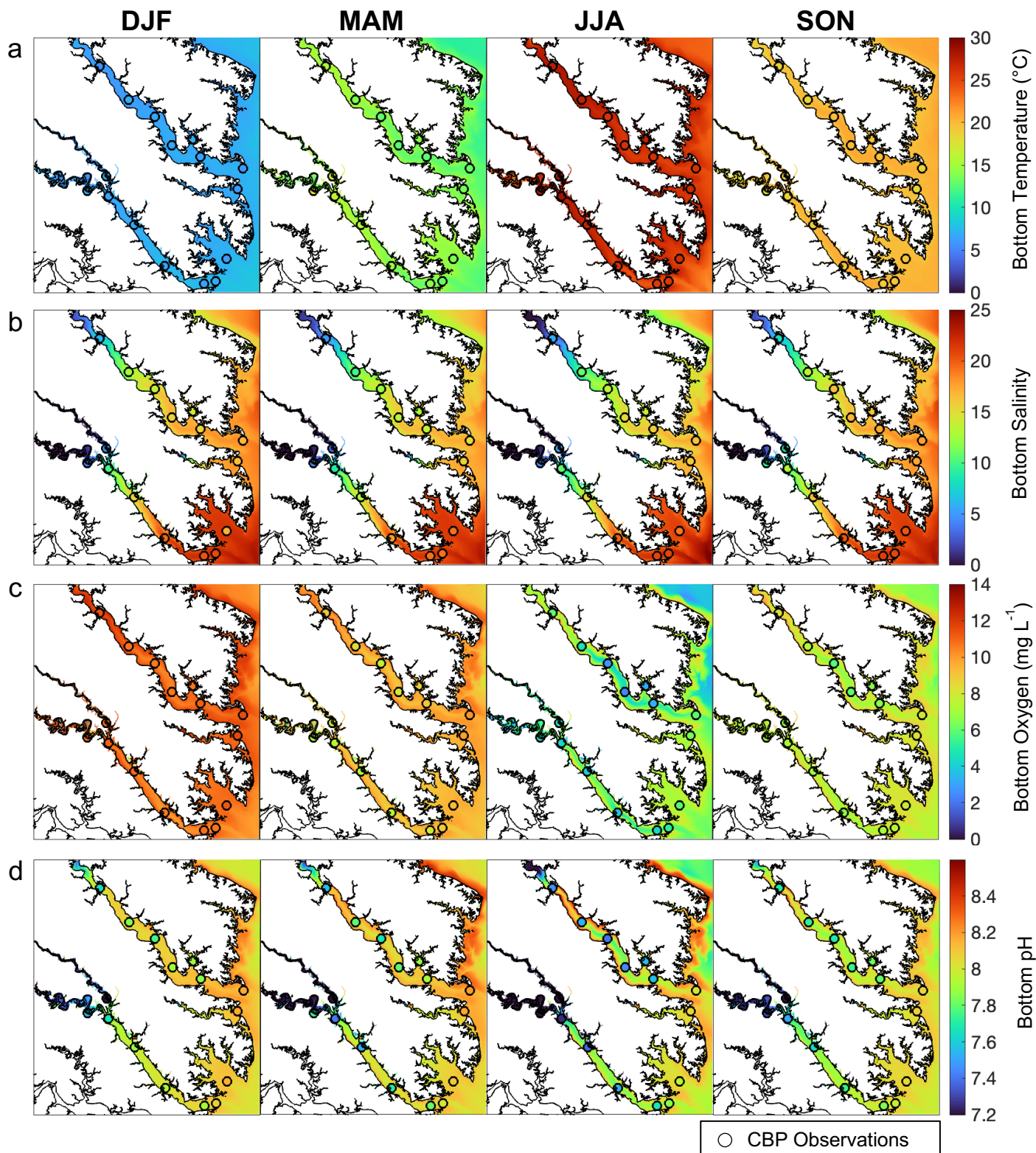
237





238

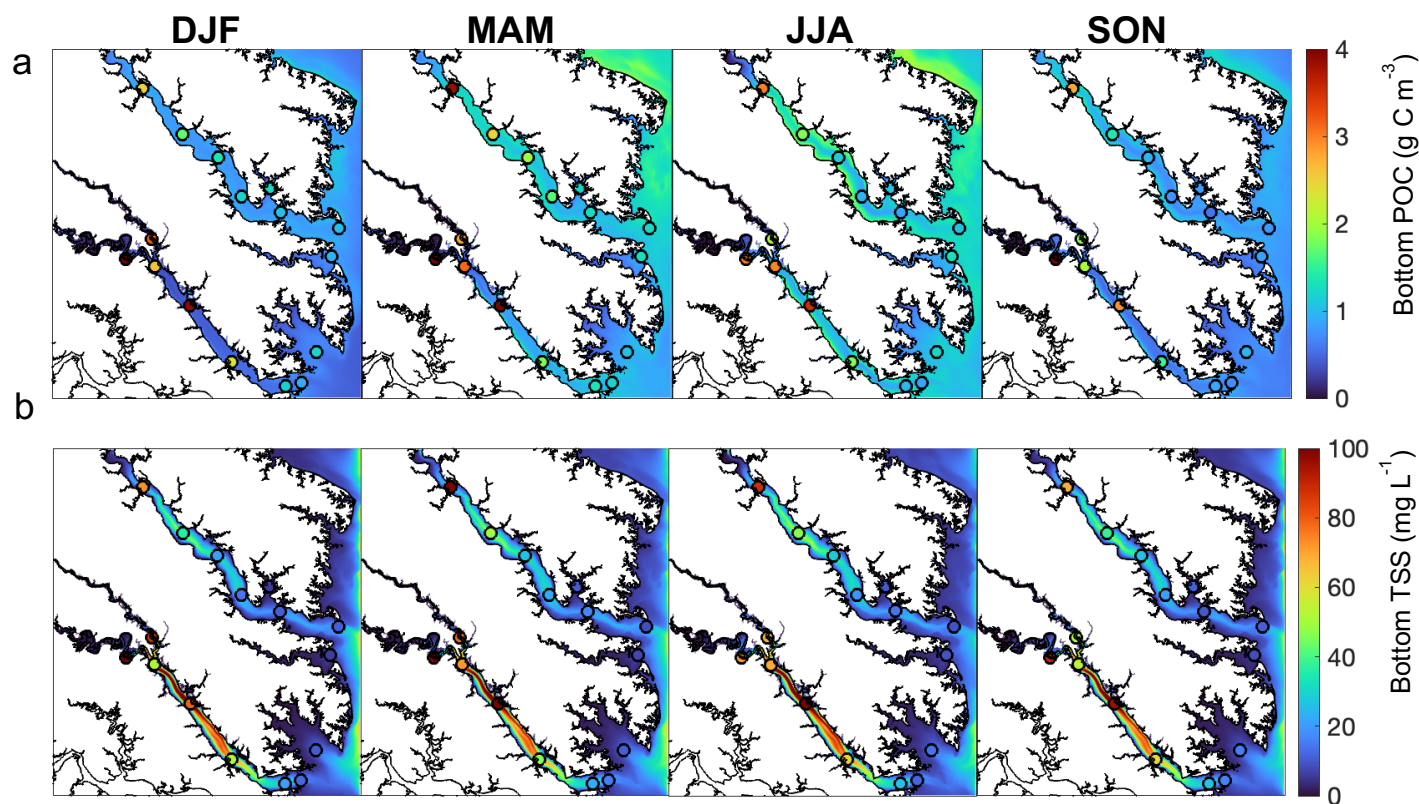
239





240 **Figure 2.** Seasonally-averaged bottom (a) temperature, (b) salinity, (c) dissolved oxygen, and (d) pH from the reference run. Circles  
241 represent seasonal decadal-averaged *in situ* observations at Chesapeake Bay Program stations (2010-2020). (DJF = winter, MAM =  
242 spring, JJA = summer, and SON = fall). Figure 1 ROMS-ECBO model domain of Chesapeake Bay tributaries illustrating (a)  
243 bathymetry in meters and locations of Chesapeake Bay Program water quality monitoring stations (red circles) and (b) bottom  
244 salinity zones.

245



246

247 **Figure 3.** Seasonally-averaged bottom (a) POC and (b) TSS from output of the reference run of the ROMS-ECBO model. Circles  
248 represent seasonal decadal-averaged bottom measurements at Chesapeake Bay Program stations (2010-2020). (DJF = winter, MAM =  
249 spring, JJA = summer, and SON = fall).

250

251 When compared to 2017 WQMP observations and seasonal decadal averages, model skill of ROMS-ECBO is  
252 reasonably high (Table 1, Figs. 2, 3), and similar to other model implementations of the Chesapeake Bay (Irby et al., 2016).  
253 Temperature and salinity are reproduced relatively well year-round (Fig. 2a,b) with annual biases of only 0.2°C and -1.5,  
254 respectively (Table 1). Bottom O<sub>2</sub> and pH are slightly overestimated, exhibiting the greatest model-data misfit in the spring  
255 and summer months in the tributary channels (Fig. 2c,d). pH is overestimated by 0.2 units, which is within the accuracy of the  
256 electrode measurements. Observed POC concentrations in the York and upper Rappahannock are higher than simulated in the



257 model and exhibit very high spatial variability (Fig. 3a). Despite the high spatial variability of the TSS observations (Fig. 3b),  
 258 mean TSS ( $45 \pm 54 \text{ mg L}^{-1}$ ) is captured within  $1.1 \text{ mg L}^{-1}$  by the model.

259 Growth rates determined using the *EcoOyster* equations and environmental outputs from ROMS-ECB were compared  
 260 with oyster data collected in the York River (Paynter et al., 2008; Liddel, 2008; Kingsley-Smith et al., 2009; Degremont et al.,  
 261 2012; Callam et al., 2016). Specifically, the tunable parameter ( $p$ ) that limits oyster filtration was adjusted to provide a best  
 262 match between the modeled oyster growth rates and the published rates. Multiple  $p$ -values were tested, and a value of  $p=0.15$   
 263 resulted in modeled oyster growth that best matched published growth rates. The resulting shell growth predicted by the model  
 264 was found to be close to the *in situ* data ( $52.0 \pm 1.1 \text{ mm y}^{-1}$  and  $51.3 \pm 2.9 \text{ mm y}^{-1}$  for the model and observation means and  
 265 standard deviations, respectively).

266 **Table 1. Model skill statistics (mean  $\pm$  standard deviation) comparing bottom grid cells from the reference run to Chesapeake Bay**  
 267 **Program observations from the same station location and time, within the bottom 10% of the water column.**

Variable	Model	Observation	Model Bias	RMSD <sup>a</sup>
Temperature (°C) n = 130	$17.0 \pm 9$	$16.7 \pm 9$	+ 0.2	0.7
Salinity n = 127	$13.9 \pm 7$	$15.4 \pm 7$	-1.5	2.7
Oxygen (mg O <sub>2</sub> L <sup>-1</sup> ) n = 130	$8.0 \pm 2.3$	$7.2 \pm 2.9$	+0.9	1.3
pH n = 74	$7.8 \pm 0.4$	$7.6 \pm 0.4$	+ 0.2	0.4
TSS (mg L <sup>-1</sup> ) n = 74	$44 \pm 34$	$45 \pm 54$	-1.1	48.3
POC (g C m <sup>-3</sup> ) n = 74	$0.7 \pm 0.3$	$1.7 \pm 2.1$	-1.0	2.4

268 <sup>a</sup>RMSD = root mean squared difference

## 269 2.4 Future simulations

270 In addition to the reference run, this study generated five future simulations (Table 2) to investigate the change in  
 271 carbonate chemistry conditions and oyster growth resulting from three drivers of future change in the bay: increased  
 272 atmospheric CO<sub>2</sub> (*AtmCO<sub>2</sub>*), atmospheric warming (*Temp*), and reduced nutrient loading (*TMDL*). Model forcings were  
 273 modified for each simulation to represent mid-century conditions. A *Combined Future* simulation was run including forcings  
 274 of all future stressors, in addition to three sensitivity simulations to isolate the impacts of each stressor on oyster growth.  
 275 Atmospheric CO<sub>2</sub> concentration for the *AtmCO<sub>2</sub>* and *Combined Future* simulations was set to 655 ppm, derived from the  
 276 Coupled Model Intercomparison Project Phase 5 report RCP8.5 (business-as-usual) scenario projected for 50 years in the



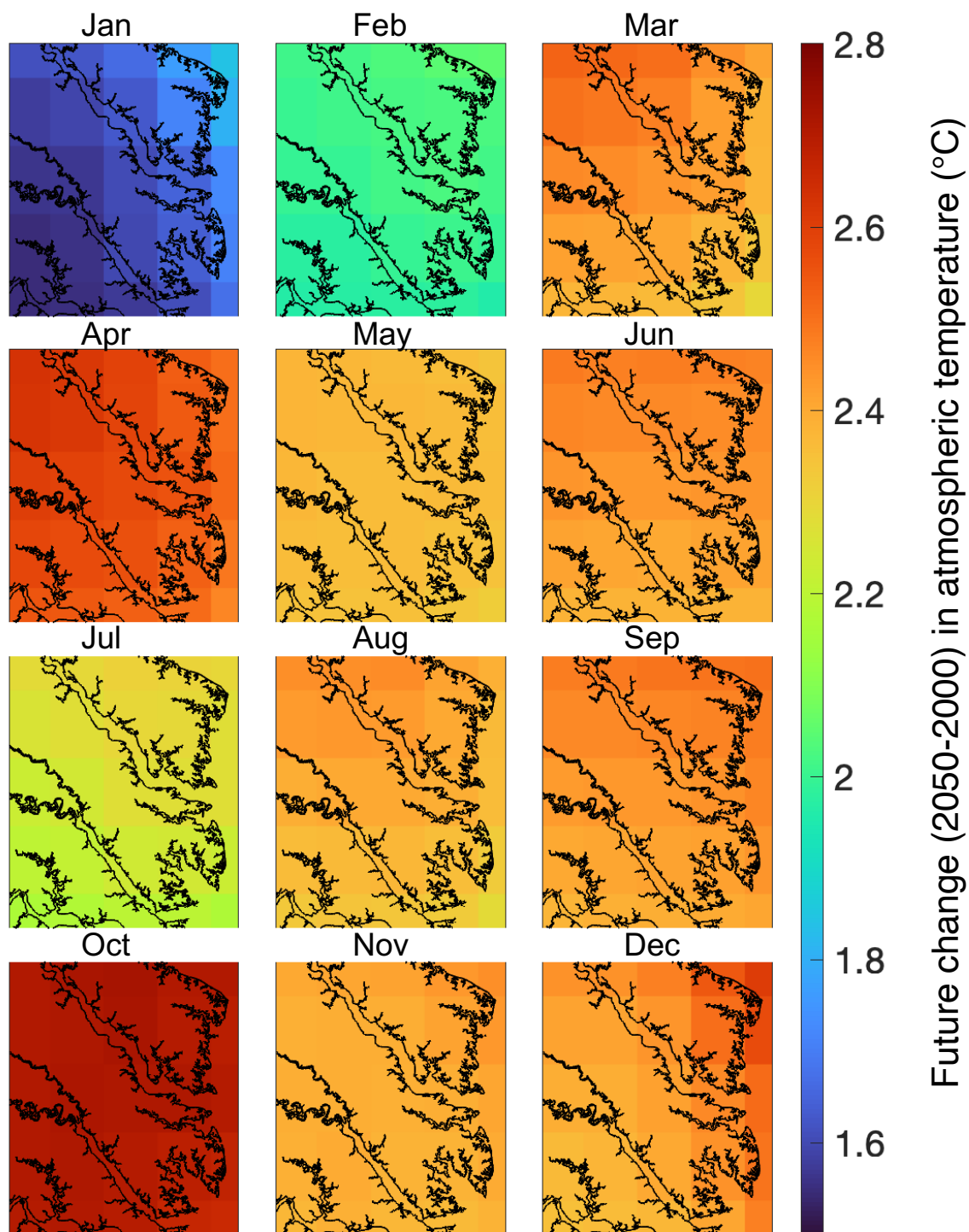
277 future relative to the reference run (Meinshausen et al., 2011). Future atmospheric temperature for the *Temp* and *Combined*  
 278 *Future* simulations was obtained from the IPSL-CM5A-LR Earth System Model (Dufresne et al., 2013), statistically  
 279 downscaled with the Multivariate Adaptive Constructed Analogs method (Abatzoglou and Brown, 2012). IPSL-CM5A-LR  
 280 was selected as in Hinson et al. (2023), since it was deemed the most representative downscaled ESM of the 20 available. As  
 281 in Hinson et al. (2023), the delta method was used to calculate the daily average change in atmospheric temperatures between  
 282 present-day and future conditions. To calculate this change, two 30-year climatologies, centered on 2000 and 2050  
 283 respectively, were computed and daily averaged 50-year differences between the two climatologies (Fig. 4) were added to the  
 284 atmospheric temperatures used in the reference run. Future watershed inputs for the *TMDL* and *Combined Future* simulations  
 285 included a climatology of nitrate, ammonium, dissolved organic matter, and particulate organic matter concentrations, derived  
 286 from a Phase 6 CBPWM 1991-2000 run using reduced nutrient concentrations assuming the TMDLs had been successfully  
 287 achieved (Bhatt et al., 2023). Freshwater discharge in this run was set to be identical to the reference run, to isolate the effects  
 288 of lowered nutrient concentrations on water chemistry and oyster growth. Since future climate change is expected to impact  
 289 terrestrial inputs much less than future management actions (Irby et al., 2018), the direct impact of climate change on the  
 290 watershed is not considered in this analysis. A fifth simulation (*AtmCO<sub>2</sub> + Temp*) was run to compare the influences of local  
 291 management actions to the combined drivers of climate change, which includes both future atmospheric CO<sub>2</sub> concentration  
 292 and atmospheric temperature. Preliminary investigations revealed a minimal impact of sea level rise on  $\Omega_{Ca}$  in the bay;  
 293 therefore, it was not included in the simulated climate change variables.

294

295 **Table 2. Experimental design for future simulations conducted for comparison to reference run. Model forcings include a**  
 296 **combination of 2017 (reference) and 2067 (future) inputs of atmospheric CO<sub>2</sub>, atmospheric temperature, and terrestrial nutrient**  
 297 **loadings.**

Future Simulation Name	Atmospheric CO <sub>2</sub>	Atmospheric Temperature	Terrestrial inputs
<b>Combined Future</b>	Future	Future	TMDL <sup>a</sup>
<b>AtmCO<sub>2</sub></b>	Future	Reference	Reference
<b>Temp</b>	Reference	Future	Reference
<b>TMDL</b>	Reference	Reference	TMDL
<b>AtmCO<sub>2</sub> + Temp</b>	Future	Future	Reference

298 <sup>a</sup>TMDL (Total Maximum Daily Load) forcing includes inputs of nitrate, ammonium, and dissolved and particulate organic  
 299 matter under the assumption that the nutrient reduction goals (EPA, 2010) are met.



300 Figure 4. Monthly-averaged 50-year atmospheric temperature differences over the ROMS-ECBO model domain calculated as  
301 projections from 2050 minus those from 2000.

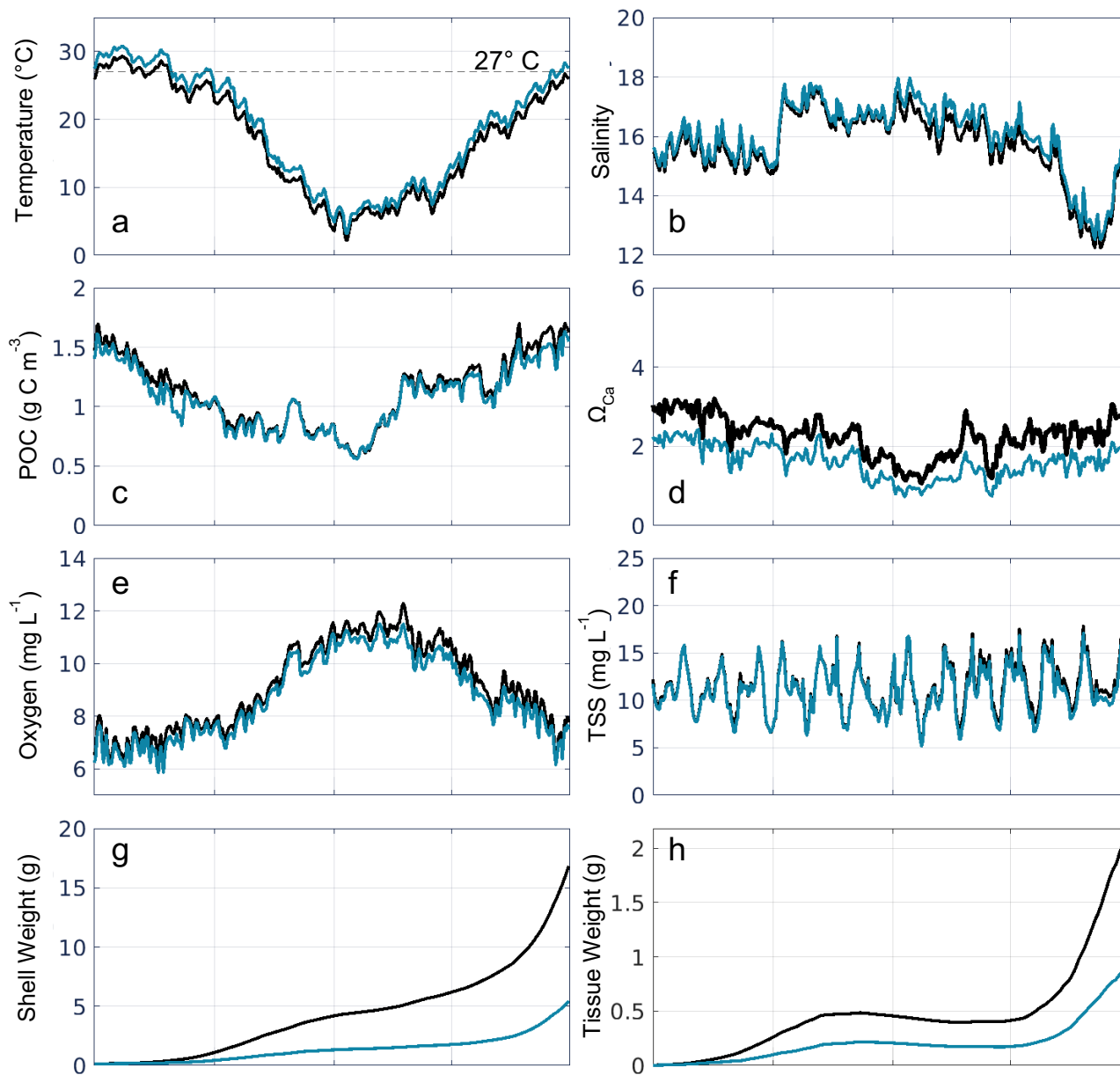


302 To generate open boundary conditions for each future simulation, a full bay model (St-Laurent and Friedrichs, 2024)  
303 was run with the same atmospheric and river forcings as in this 120-meter model implementation. As in the reference run, all  
304 future simulations were spun up for six months (January 1 – June 30) before beginning on July 1, but represent 50 years in the  
305 future from the reference simulation (i.e., July 1, 2067). Initial conditions for all spin-ups are identical to the reference  
306 simulation. Analysis confirmed the effects of initial conditions are negligible by July 1. To examine results most relevant to  
307 oysters, model output was extracted at locations that support oyster production, defined as all grid cells in which tissue weight  
308 exceeded 1 g at the end of the reference run (i.e., one year of growth; Fig. S2). All results shown are from the bottom level of  
309 the model, representing conditions similar to on-bottom or bottom cage aquaculture methods that are common in Virginia.  
310 Spatial variation in model outputs across grid cells in the model domain is reported using standard deviation.

## 311 3 Results

### 312 3.1 Reference run results

313 In the present-day reference run, the environmental variables used as inputs to the oyster parameterizations exhibit  
314 substantial seasonal (Fig. 5a-f) and spatial (Figs. 6, S3) variability. As expected, bottom temperature is highest in summer,  
315 reaching an average of 29.3 °C in July when averaged across grid cells that support oyster growth (Fig. 5a). Temperature is  
316 higher in the shallower parts of the tributaries compared to the channels (Fig. S3a). Bottom salinity exhibits higher values in  
317 the fall and winter, reaching a maximum average of 17.7 in October, and drops in the spring and summer to reach a minimum  
318 average of 12.3 in June (Fig. 5b). Annual average bottom salinity ranges from 0 to 26 throughout the model domain (Fig. S3b),  
319 with the highest values in the southern areas in closest proximity to the open-ocean. The seasonal cycle for bottom POC is  
320 similar to that of temperature, peaking at 1.7 g C m<sup>-3</sup> in June and dropping to 0.57 g C m<sup>-3</sup> in January (Fig. 5c). Bottom POC  
321 also varies widely throughout the model domain (Fig. 6a), with relatively higher values in the Rappahannock compared to the  
322 York River, along the shoals of the tributaries, and along the western shoals of the mainstem Bay north of the Rappahannock.  
323  $\Omega_{Ca}$  exhibits an annual cycle similar to that of temperature and POC, reaching a maximum average of 3.2 in August and a  
324 minimum average of 1.1 in January. Annual mean bottom  $\Omega_{Ca}$  also varies widely throughout the model domain (Fig. 6d).  
325 Generally, bottom  $\Omega_{Ca}$  increases with salinity, with low to zero values in the tidal fresh portions of the upper tributaries and  
326 higher values along the western shoals of the mainstem Chesapeake Bay. The opposite temporal pattern is seen in bottom O<sub>2</sub>,  
327 which peaks at 12.3 mg L<sup>-1</sup> in February and drops to an average of 6.3 mg L<sup>-1</sup> in August (Fig. 5e). O<sub>2</sub> concentrations are highest  
328 along the shoals and lowest in the deep channels (Fig. S3c). Bottom TSS concentrations exhibit tidal variability throughout  
329 the year and are highest in the York River with much lower concentrations observed in the other portions of the model domain  
330 (Fig. S3d). Environmental conditions averaged annually across grid cells that support oyster growth are provided in Table 3,  
331 and conditions averaged annually across all grid cells in the model domain are provided in Table S5.



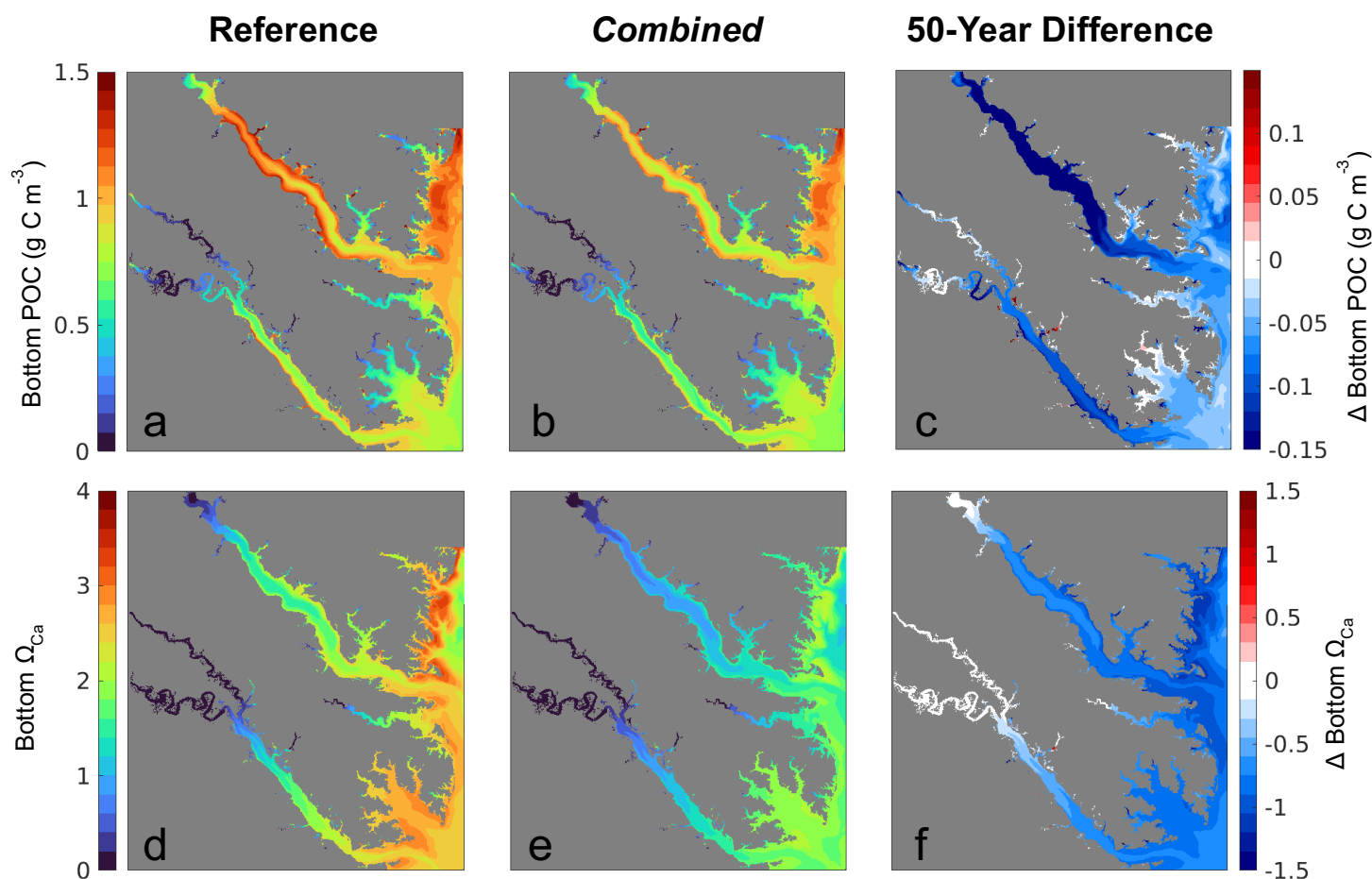
332

333 **Figure 5. Time series of daily bottom (a) temperature, (b) salinity, (c) POC, (d) Ω<sub>Ca</sub>, (e) shell weight, and (f) tissue weight, averaged**  
334 **over grid cells that support oyster growth in the reference run, for the present-day reference run (black line) and Combined Future**  
335 **simulation (blue line).**

336



337



338 **Figure 6.** Annual mean bottom (a-c) POC and (d-f)  $\Omega_{Ca}$  from (a,d) the present-day reference run, (b,e) the *Combined Future*  
339 simulation, and (c,f) the difference between (a) and (b), i.e., *Combined Future* minus reference.

340

341 Tissue and shell weights increase modestly from July through April, and the highest rates of increase are seen in May  
342 and June near the end of the one-year reference run (Fig. 5g,h). At the end of the reference run, the spatial patterns of shell and  
343 tissue weight are nearly identical (Fig. 7), as tissue growth largely drives shell growth (Table S4). Both shell and tissue weights  
344 are highest along the shoals of the York and Rappahannock Rivers (Fig. 7a,d) and low in the deeper waters where TSS  
345 concentrations are high (Fig. S3d). A wider region of high shell and tissue weight appears in the Rappahannock, while the  
346 highest weights in the York are confined to a very narrow and shallow strip along the coastline. Shell and tissue weights are  
347 higher along the southwestern than the northeastern coastlines of the tributaries, where the shoals are wider in both tributaries  
348 (Fig. 1a). Oyster growth metrics averaged across grid cells that support oyster growth are provided in Table 4.





349 **Table 3. Bottom environmental variables for each model simulation (annual mean  $\pm$  standard deviation) for grid cells that support**  
 350 **oyster growth in the reference run (defined as those with greater than 1g dry tissue weight after one year of growth; Fig. S2).**  
 351 **Analogous results averaged over all model grid cells are shown in Table S5.**

Model Simulation	Temperature (°C)	Salinity	POC (g C m <sup>-3</sup> )	$\Omega_{Ca}$	Dissolved Oxygen (mg O <sub>2</sub> L <sup>-1</sup> )	TSS (mg L <sup>-1</sup> )
Reference	17.0 $\pm$ 0.7	15.7 $\pm$ 2.1	1.12 $\pm$ 0.1	2.5 $\pm$ 0.49	9.1 $\pm$ 0.6	11.4 $\pm$ 5.8
Combined Future	18.5 $\pm$ 0.8	16.0 $\pm$ 2.1	1.03 $\pm$ 0.1	1.6 $\pm$ 0.35	8.7 $\pm$ 0.6	11.1 $\pm$ 5.9
AtmCO <sub>2</sub>	17.0 $\pm$ 0.7	15.7 $\pm$ 2.1	1.12 $\pm$ 0.1	1.6 $\pm$ 0.35	9.1 $\pm$ 0.6	11.4 $\pm$ 5.8
Temp	18.5 $\pm$ 0.8	16.0 $\pm$ 2.1	1.07 $\pm$ 0.1	2.5 $\pm$ 0.41	8.8 $\pm$ 0.6	11.1 $\pm$ 5.9
TMDL	17.0 $\pm$ 0.7	15.7 $\pm$ 2.1	1.08 $\pm$ 0.1	2.4 $\pm$ 0.53	9.1 $\pm$ 0.6	11.2 $\pm$ 5.9
Temp + CO <sub>2</sub>	18.5 $\pm$ 0.8	16.0 $\pm$ 2.1	1.07 $\pm$ 0.1	1.7 $\pm$ 0.33	8.8 $\pm$ 0.6	11.1 $\pm$ 5.9

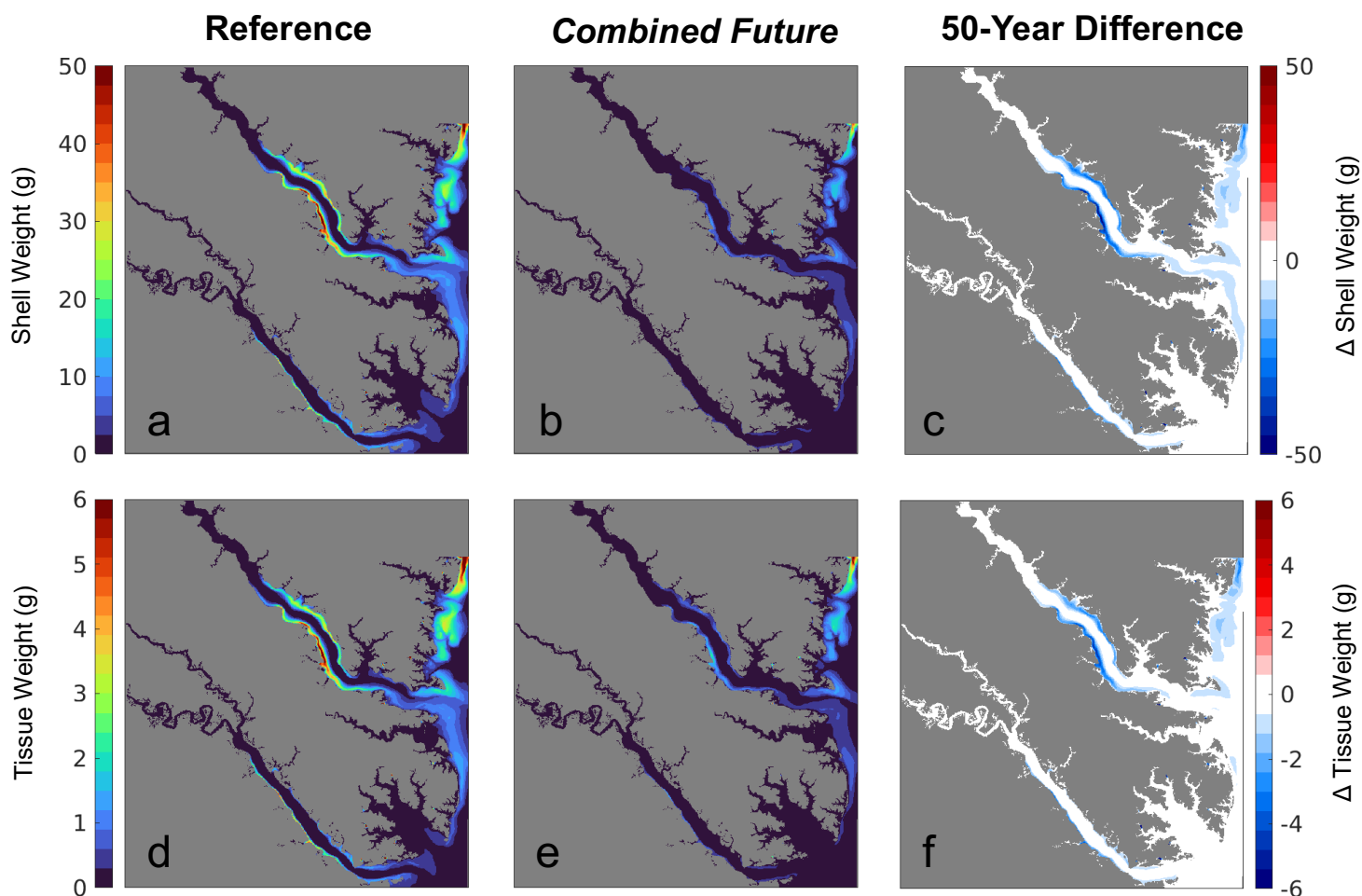
352

353 **Table 4. Modeled oyster characteristics from the end of each simulation (mean  $\pm$  standard deviation) over grid cells that support**  
 354 **oyster growth in the reference run (defined as those with greater than 1g dry tissue weight after one year of growth; Fig. S2).**

Model Simulation	Shell Weight (g)	Tissue Weight (g)	Shell Thickness (g mm <sup>-1</sup> )
Reference	16.8 $\pm$ 10.9	2.2 $\pm$ 1.5	0.18 $\pm$ 0.08
Combined Future	5.4 $\pm$ 5.7	0.9 $\pm$ 0.8	0.07 $\pm$ 0.05
AtmCO <sub>2</sub>	10.5 $\pm$ 8.0	2.2 $\pm$ 1.5	0.12 $\pm$ 0.06
Temp	9.7 $\pm$ 9.1	1.2 $\pm$ 1.1	0.10 $\pm$ 0.07
TMDL	13.1 $\pm$ 8.2	1.7 $\pm$ 1.2	0.15 $\pm$ 0.06
Temp + CO <sub>2</sub>	6.6 $\pm$ 7.1	1.2 $\pm$ 1.1	0.08 $\pm$ 0.06



355



356 **Figure 7.** (a-c) Shell weight and (d-f) tissue weight at the end of the one-year simulation from (a,d) the present-day reference run,  
357 (b,e) the *Combined Future* run, and (c,f) their difference, i.e., *Combined Future* minus reference.

### 358 **3.2 Results of Combined Future simulation**

359 All environmental variables examined exhibit change from the reference run in the *Combined Future* simulation.  
360 Temperature and salinity are projected to increase across the entire model domain (Fig. S3a,b). When averaged over the model  
361 domain, temperature is projected to increase by  $1.5 \pm 0.26^\circ\text{C}$ , and salinity is projected to increase by  $0.21 \pm 0.11$  (Table S5).  
362 Bottom POC is projected to decrease by  $0.07 \pm 0.05 \text{ g C m}^3$  (Table S5), with POC reductions predicted to be most pronounced  
363 in the mid- to upper tributaries (Fig. 6c). Mid-century bottom  $\Omega_{\text{Ca}}$  is projected to be lower throughout most of the region,  
364 with an average reduction of  $0.8 \pm 0.19$  over the whole model domain (Table S5). The spatial distribution of future  $\Omega_{\text{Ca}}$  is generally  
365 consistent with present-day  $\Omega_{\text{Ca}}$  patterns, and the greatest decreases are projected to occur in regions with the highest present-



366 day  $\Omega_{ca}$  (Fig. 6 d,e,f). An average reduction in  $O_2$  of  $0.3 \pm 0.08 \text{ mg L}^{-1}$  is predicted across the model domain (Table S5), which  
367 will be mostly spatially uniform (Fig. S3c). TSS is projected to be reduced by  $0.20 \pm 0.25 \text{ mg L}^{-1}$  with high spatial variability  
368 in the projected change (Fig. S3d).

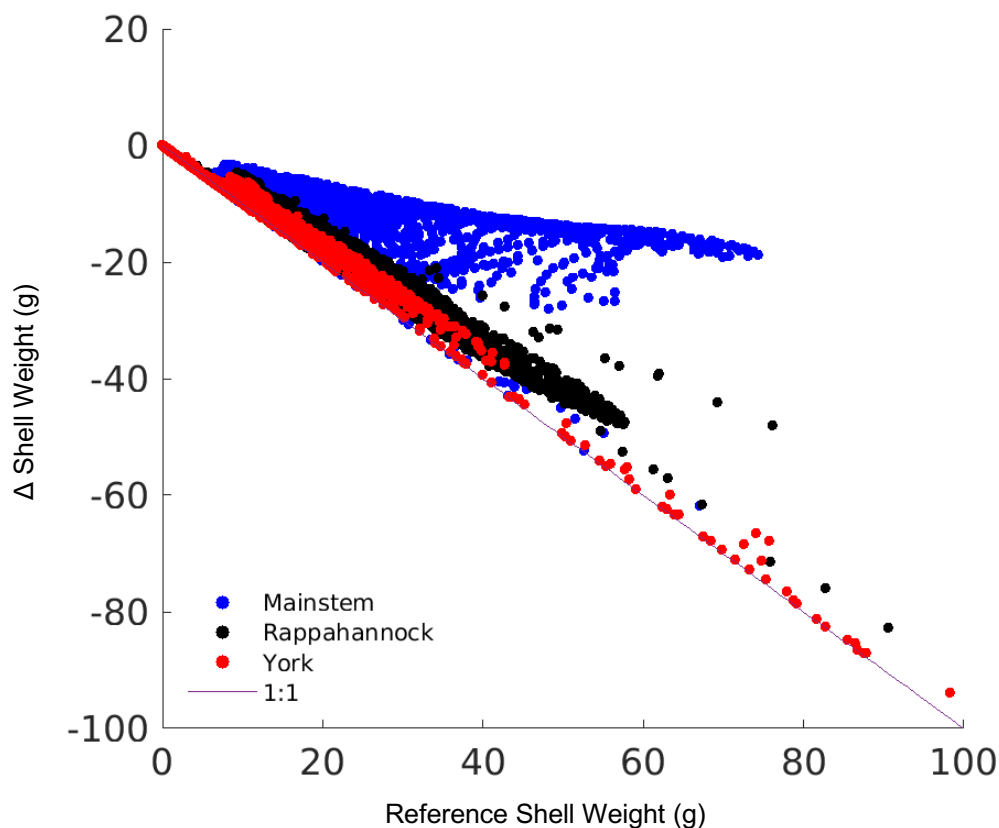
369 Changes in environmental conditions do not occur uniformly throughout the year. Temporal changes in environmental  
370 conditions averaged across grid cells that support oyster growth are provided in Figure 5. Annually averaged increases in  
371 temperature and salinity are the same when averaged over only grid cells that support oyster growth as they are when averaged  
372 across the entire model domain (Tables 3, S5). The greatest temperature increases are projected to occur in the warmer months,  
373 with an average increase of  $1.6 \text{ }^\circ\text{C}$  predicted for June through August and an average increase of  $1.2 \text{ }^\circ\text{C}$  predicted for December  
374 through February. Bottom temperatures are projected to surpass the optimal temperature for oyster filtration ( $27 \text{ }^\circ\text{C}$ ) primarily  
375 in July and August (Fig. 5a). Salinity increases are projected to be greatest at the beginning of the year, with an average increase  
376 of  $0.44$  between January and March and an average increase of  $0.20$  for the remainder of the year (Fig. 5b). Bottom POC at  
377 grid cells that support oyster growth is expected to decrease slightly less than the average for the entire region (Tables 3, S5),  
378 with the greatest reductions in the spring and summer and little to no change in the winter (Fig. 5c). For  $\Omega_{ca}$ ,  $O_2$ , and TSS,  
379 projected reductions are slightly greater at oyster growth sites than for the entire domain.  $\Omega_{ca}$  is projected to decrease by  $0.9$ ,  
380 with the greatest reductions expected to occur the warmer months (Fig. 5d).  $O_2$  is projected to decrease year-round, though  
381 with slightly greater reductions in the winter (Fig. 5e) and an annual average reduction of  $0.4 \text{ mg } O_2 \text{ L}^{-1}$  (Table 3). TSS is  
382 projected to decrease annually by  $0.3 \text{ mg L}^{-1}$  (Table 3), mostly in the spring, due to lowered POC (Fig. 5f).

383 Modeled shell and tissue weights after one year of growth are projected to decline in all regions that exhibit present-  
384 day growth, with the most severe reductions (up to 100%) occurring along the York and Rappahannock River shoals (Figs.  
385 7c,f, 8). One-year tissue weight will be reduced by  $1.3 \text{ g}$ , on average, representing a 60% reduction across grid cells that support  
386 oyster growth (Table 4). Shell weight, which is largely driven by changes in tissue weight, is projected to be reduced by  $11.4$   
387 g on average after one year of growth, representing a 68% reduction in average shell weight in regions that support oyster  
388 growth (Table 4). The greatest reduction in shell and tissue growth rates will occur in the warmer months near the end of the  
389 one-year simulation ( $-0.1 \text{ g d}^{-1}$  from May through June), whereas the smallest change will occur in the winter months ( $-0.02 \text{ g}$   
390  $\text{d}^{-1}$  from December through February), as the least growth occurs during that time (Fig. 5g,h). Shell thickness, calculated as  
391 the ratio of shell weight to shell height, will be reduced by 61% on average ( $0.11 \text{ g mm}^{-1}$ ; Table 4).

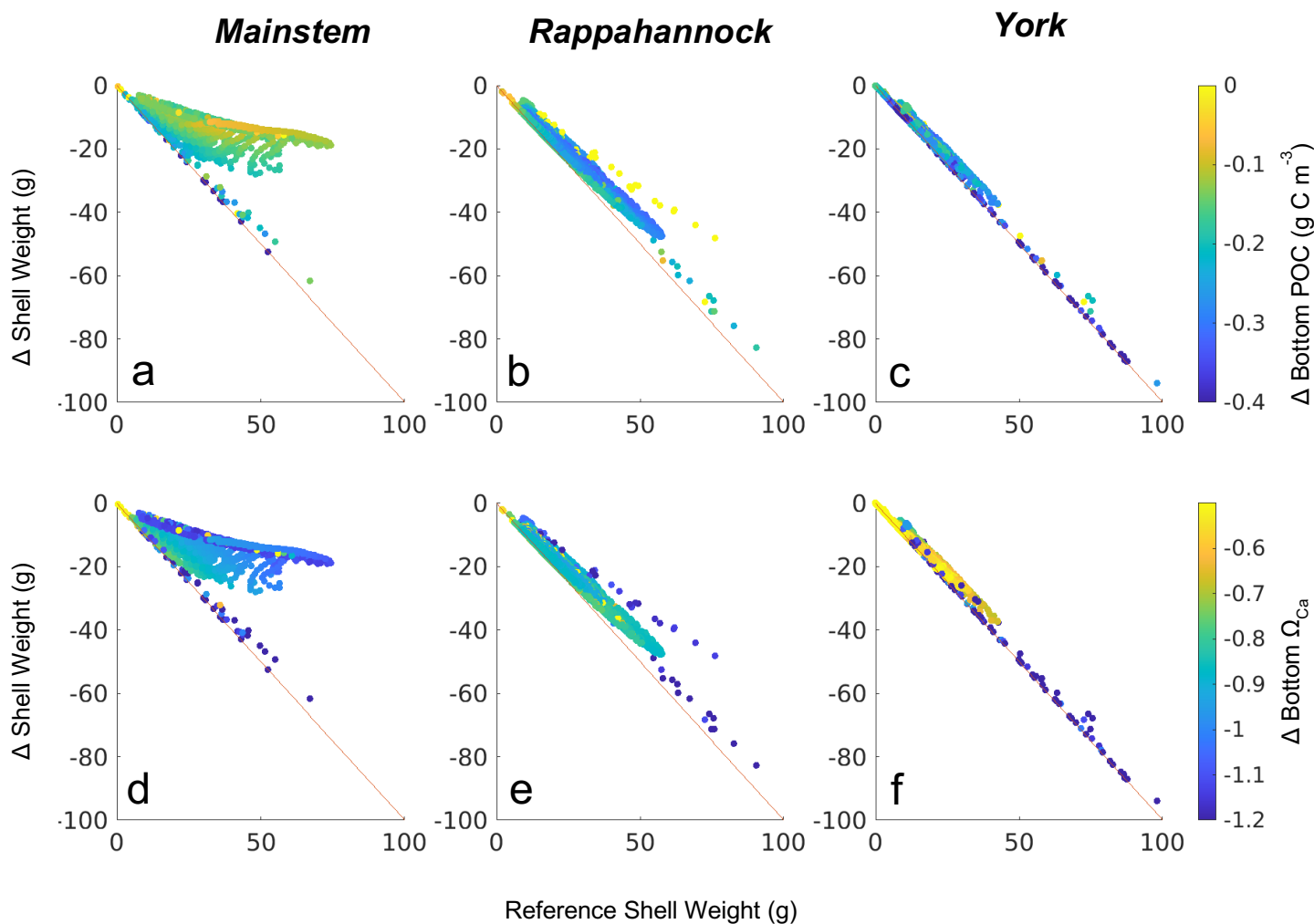
392 Declines in year one shell weight will vary throughout the model domain (Fig. 8), following relative changes in  
393 bottom POC and  $\Omega_{ca}$  (Fig. 9). The mainstem has the most moderate reduction in shell weight relative to reference shell weight,  
394 with an average reduction of 31%, indicated by the slope of the scatterplot. Shell weights in the Rappahannock and York face  
395 the steepest reductions relative to reference, with average reductions of 86% and 96%, respectively, and a large portion of  
396 York oysters facing complete depletion of oyster tissue and shell in these locations (Fig. 9; indicated by proximity to 1:1 line).  
397 Proportional shell weight reductions in the mainstem are projected to correlate with POC reductions (Fig. 9a). For  $\Omega_{ca}$  in the  
398 mainstem, a group of sites face the greatest proportional reductions when  $\Omega_{ca}$  reductions are the greatest. However, for sites  
399 with lower proportional shell loss, the opposite trend is observed (Fig 9d). In the Rappahannock, higher POC reductions



400 coincide with slightly lower proportional shell loss (Fig. 9b). Sites with the largest reductions in POC primarily occur in the  
401 York (Fig. 9c; see dark blue symbols on the 1:1 line), and the greatest proportional shell weight reductions coincide with the  
402 greatest POC and  $\Omega_{Ca}$  reductions (Fig. 9c,f). Similar results are found for tissue weight (not shown).



403  
404 **Figure 8. Difference in shell weight at the end of the one-year simulation between the *Combined Future* run and the reference run,**  
405 **i.e., *Combined Future* minus reference, colored by region. Each point represents a grid cell where oyster growth occurs in the**  
406 **reference run.**



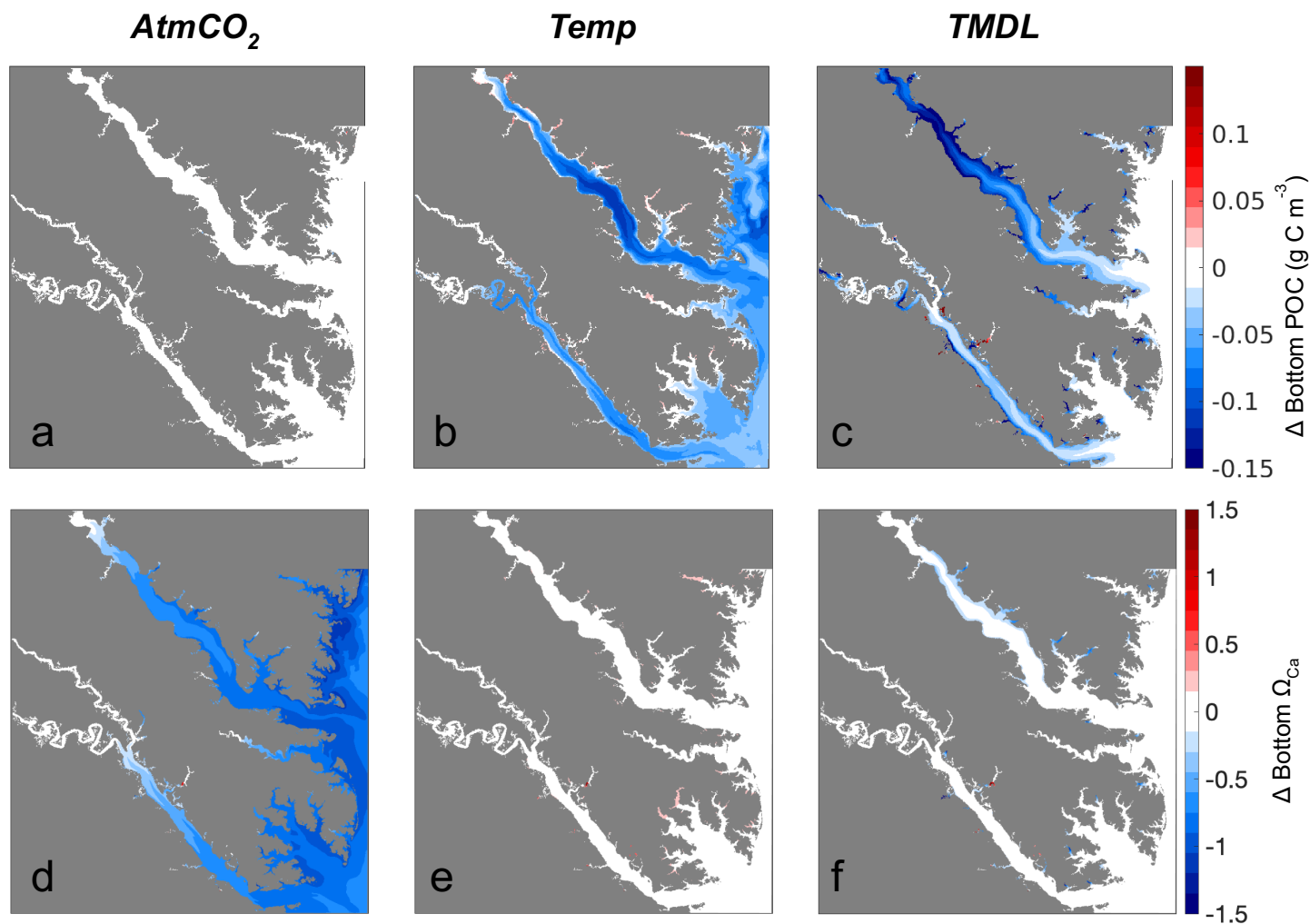
407 **Figure 9.** Difference in shell weight at the end of the one-year simulation between the *Combined Future* run and the reference run  
408 colored by (a-c) change in POC and (d-f) change in bottom  $\Omega_{Ca}$  (i.e. *Combined Future* minus reference) for grid cells that support  
409 oyster growth. Results are presented for (a,d) the mainstem shoal only, (b,e) the Rappahannock River only, and (c,f) the York River  
410 only.

### 411 3.3 Results of individual future sensitivity simulations

412 Four individual future sensitivity simulations were conducted to isolate the specific mechanisms (increased  
413 atmospheric  $CO_2$ , increased atmospheric temperature, and/or nutrient reductions) causing the projected changes described  
414 above in the *Combined Future* simulation. The *AtmCO<sub>2</sub>* sensitivity simulation produces substantial reductions in average  
415 bottom  $\Omega_{Ca}$  (Fig. 10d) and, as expected, is not projected to substantially impact bottom temperature, salinity, POC,  $O_2$ , or TSS  
416 (Table 3; Figs. 10a, S4). The projected reduction in  $\Omega_{Ca}$  is 0.9 when averaged over oyster growth sites (Table 3), 0.1 greater in  
417 magnitude than the average reduction for the entire model domain (Table S5), as greater reductions are expected along the  
418 shoals of the Rappahannock and mainstem shoal than the York and upper section of the Rappahannock (Fig. 10d). In this

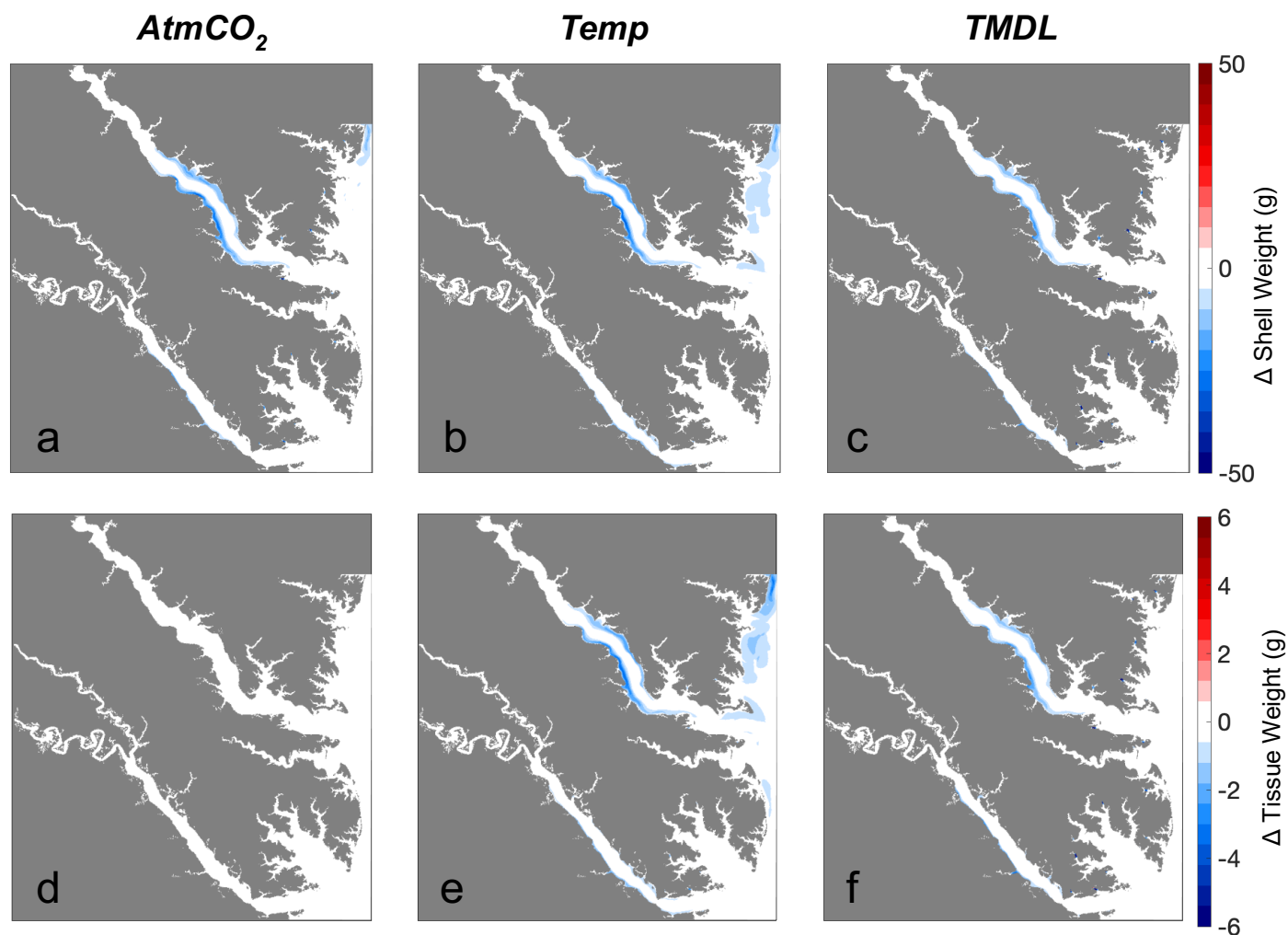


419 *AtmCO<sub>2</sub>* simulation, shell weight is predicted to be most steeply reduced in the Rappahannock, with less impact in the York  
420 and mainstem regions (Fig. 11a). At grid cells with oyster growth, *AtmCO<sub>2</sub>* produces a shell weight reduction of 6.3 g in  
421 comparison to the reference simulation, but no change in tissue weight (Table 4).  
422



423 **Figure 10. Differences in annual averaged (a-c) bottom POC and (d-f) bottom  $\Omega_{Ca}$  (d-f) for three sensitivity experiments: (a)**  
424 ***AtmCO<sub>2</sub>*, (b) *Temp*, and (c) *TMDL*. Differences represent future results minus those from the present-day reference run.**

425



426 **Figure 11 Differences in (a-c) shell weight and (d-f) tissue weight at the end of the one-year simulation for three sensitivity**  
427 **experiments: (a) *AtmCO<sub>2</sub>*, (b) *Temp*, and (c) *TMDL*. Differences represent future results minus those from the present-day reference**  
428 **run.**

429 The *Temp* sensitivity simulation produces changes in all environmental variables impacting oyster growth, with the  
430 exception of  $\Omega_{Ca}$  (Tables 3, S5). Average changes in temperature, salinity, and TSS will be identical to those from the  
431 *Combined Future* simulation (Tables S5, 3). Predicted reductions in POC and O<sub>2</sub> will be smaller in magnitude than in  
432 *Combined Future*, though more severe than any other single sensitivity experiment (Table 3). Temperature and salinity will  
433 increase across the entire model domain, with a greater salinity increase occurring in the Rappahannock and along the mainstem  
434 shoal (Fig. S4a-c). TSS will decrease primarily in the channels of the lower York and Rappahannock and on the mainstem  
435 shoal (Fig. S4d). POC reductions are expected to cover the majority of the model domain, with larger reductions in the upper  
436 Rappahannock (Fig. 10b). Slight increases in  $\Omega_{Ca}$  are observed in shallow tidal creeks (Fig. 10e); however, no substantial



437 change in average  $\Omega_{Ca}$  is predicted (Table 3, S5).  $O_2$  at oyster grid cells will exhibit a similar but slightly smaller average  
438 reduction compared to *Combined Future* (Table 3). Patterns of change in shell weight in the *Temp* sensitivity simulation  
439 resemble those in the *AtmCO<sub>2</sub>* simulation (Fig. 11b), with additional reductions along the mainstem shoal and a greater  
440 predicted mean reduction of 7.1 g, a 42% decrease at grid cells with oyster growth (Table 4). Unlike *AtmCO<sub>2</sub>*, tissue weight  
441 will decrease in *Temp*, by an average of 1 g, a 46% reduction (Table 4).

442 The *TMDL* sensitivity simulation produces a much smaller average change in environmental conditions than the  
443 *AtmCO<sub>2</sub>* or *Temp* simulations (Tables S5, 3). *TMDL* does not substantially influence temperature, salinity, or  $O_2$  (Tables S5,  
444 3, Fig. S4), but produces POC and TSS reductions close to the averages for *Temp* (Tables S5, 3). While POC change in the  
445 *Temp* simulation is concentrated in the deeper portions of the tributaries (Fig. 10b), the POC reductions in the *TMDL* simulation  
446 are concentrated along the shoals of the tributaries, with the greatest reductions in the upper Rappahannock (Fig. 10c). TSS  
447 changes in *TMDL* are limited to the tributaries, occurring along the shoals of the Rappahannock and in patches throughout the  
448 York (Fig. S4d). Future change in  $\Omega_{Ca}$  in this simulation is less than for *AtmCO<sub>2</sub>* and is largely confined to the upper  
449 Rappahannock shoals and in shallow tidal creeks throughout the study region (Fig. 10f). Patterns of change in shell weight  
450 will resemble *AtmCO<sub>2</sub>* and *Temp* in the tributaries, but no change is predicted along the mainstem shoal (Fig. 11c). The *TMDL*  
451 simulation produces reduced shell (3.7 g) and tissue (0.5 g) weights, with a smaller negative influence on shell and tissue  
452 weight than *Temp* (Table 4; Fig. 11c, d).

453 Environmental conditions in the *AtmCO<sub>2</sub>* + *Temp* simulation are nearly identical to those in the *Combined Future*  
454 simulation (Tables 3, S5), with the exception of  $\Omega_{Ca}$ , which is slightly higher due to the absence of *TMDL*'s influence. As tissue  
455 growth is unaffected by  $\Omega_{Ca}$ , tissue weight in this simulation is identical to that of the *Temp* simulation. Average shell weight  
456 reduction in *AtmCO<sub>2</sub>* + *Temp* is 10.2 g, slightly greater than from *AtmCO<sub>2</sub>* alone, due to the combined influences of lowered  
457 tissue growth and lower  $\Omega_{Ca}$ .

#### 458 **4 Discussion**

459 This study provides high-resolution projections for oyster growing conditions and corresponding oyster growth in the  
460 Chesapeake Bay, with a specific focus on two Virginia tributaries. A high-resolution hydrodynamic-biogeochemical model  
461 was coupled with an Eastern oyster bioenergetics model and forced with future projections for atmospheric  $CO_2$ , temperature,  
462 and nutrient management. An overall reduction in  $\Omega_{Ca}$  and oyster growth are predicted by mid-century throughout the study  
463 region under the combined effects of all three future stressors. Specifically, the greatest reductions in oyster growth are  
464 projected to occur in the York and Rappahannock Rivers, where unfavorable conditions for calcification will expand in the  
465 future and where food availability will be strongly impacted by warming and nutrient reductions. Bottom conditions in the  
466 York and Rappahannock rivers, particularly in the upper portions, will likely be unsuitable for aquaculture at mid-century on  
467 average, indicating climate change preparedness is critical for the oyster aquaculture industry.





#### 468 4.1 Future projections of $\Omega_{Ca}$

469 The magnitude of future change in  $\Omega_{Ca}$  varies with present-day  $\Omega_{Ca}$  conditions. Regions with high present-day  $\Omega_{Ca}$ ,  
470 primarily the mainstem shoals, are projected to experience the greatest reductions because of their low partial pressure of  $CO_2$   
471 ( $pCO_2$ ) relative to fresher waters. Biologically driven low  $pCO_2$  water on mainstem shoals has a greater capacity for  $CO_2$   
472 uptake from the atmosphere than high  $pCO_2$  water, which is causing the fresher tributaries to experience smaller increases in  
473 DIC and smaller reductions in  $\Omega_{Ca}$ . Acidic freshwater input often causes  $pCO_2$  in the upper tributaries to exceed atmospheric  
474  $pCO_2$ , causing outgassing (Cai et al., 2017; Shen et al., 2019b; St-Laurent et al., 2020; Cai et al., 2021). Despite the lower  
475 Rappahannock having a lower salinity than the lower York, it also has a lower DIC to TA ratio, so the rate at which the lower  
476 Rappahannock absorbs  $pCO_2$  is higher (Da et al., 2021). Total alkalinity, or buffering capacity, is also lower in the lower  
477 Rappahannock than the lower York, so the lower Rappahannock cannot resist changes in carbonate chemistry to the same  
478 degree as the York. As a result, we observe the Rappahannock changing faster than the York. Since higher  $\Omega_{Ca}$  regions will  
479 experience greater reductions than lower  $\Omega_{Ca}$  regions (Fig. 5), the overall spatial variability of  $\Omega_{Ca}$  will be reduced by mid-  
480 century, and more areas will experience conditions that are unfavorable for oyster shell-building.

481 Although future atmospheric  $CO_2$  and reduced nutrient loading will both contribute to  $\Omega_{Ca}$  reductions, the modeling  
482 experiments conducted here highlight that increasing atmospheric  $CO_2$  is the largest contributor to decreases in  $\Omega_{Ca}$  throughout  
483 the study region. Increased atmospheric  $CO_2$  will cause reductions in  $\Omega_{Ca}$  across the model domain, while nutrient reductions  
484 are expected to mainly influence  $\Omega_{Ca}$  in shallow and fresh coastal areas, with little influence in oyster growing regions. The  
485 effects of warming on  $\Omega_{Ca}$  may slightly offset the influence of atmospheric  $CO_2$  in certain areas, but this will likely only occur  
486 in fresh tidal creeks where oysters do not currently reside (Fig. 10e). Given the importance of atmospheric  $CO_2$  in shaping  
487 future  $\Omega_{Ca}$  conditions in the lower bay, reductions in anthropogenic carbon emissions will be necessary to lessen the projected  
488 impacts on carbonate chemistry in the Chesapeake Bay and globally.

489 Comparing our results to other studies examining the effects of acidification reveals that the Chesapeake Bay will  
490 likely acidify faster than the US West Coast. Siedlecki et al. (2021a) projected a decrease of 0.8-1.0 in  $\Omega_{Ca}$  in the Northern  
491 California Current System between 2000 and 2100. Projections from the present work indicate a similar magnitude of reduction  
492 in the lower Chesapeake Bay over a shorter time period (50 years), suggesting a faster rate of acidification in the lower bay.  
493 Feely et al. (2009) also reported that projections for  $\Omega_{Ca}$  reductions are slightly greater in the Atlantic than in the Pacific. The  
494 relative differences in rates of acidification should be considered, however, in the context of present-day  $\Omega_{Ca}$ . The Pacific  
495 Ocean has a higher ratio of DIC:TA than the Atlantic, so present-day Pacific  $\Omega_{Ca}$  is lower (Feely et al., 2004; Dunne et al.,  
496 2012). Therefore, while the Chesapeake Bay is acidifying faster, coastal Pacific waters may become undersaturated with calcite  
497 and aragonite sooner than in Chesapeake Bay. US West Coast shellfish mortality events associated with acidification or other  
498 climate change stressors may place increased pressure on US Atlantic fisheries to provide shellfish to the nation, highlighting  
499 the importance of climate change preparedness and resilience in the Chesapeake Bay region.



500 While atmospheric CO<sub>2</sub> is primarily responsible for changes in  $\Omega_{Ca}$ , nutrient reductions are also projected to worsen  
501 carbonate chemistry conditions. Eutrophication can suppress acidification by increasing primary production (Borges and  
502 Gypens, 2010; Shen et al., 2019; Da et al., 2021), and when simulating a reduction in eutrophication via nutrient management  
503 in our modeling study, the countering effect occurred. While the reduction in  $\Omega_{Ca}$  from nutrient management is minor compared  
504 to the projected impacts of CO<sub>2</sub>-driven acidification, its small contribution may shift  $\Omega_{Ca}$  conditions from favoring net  
505 calcification to favoring net dissolution, demonstrating the importance of considering multiple drivers when predicting  
506 exposure to ecologically relevant conditions of coastal acidification.

#### 507 4.2 Future projections of oyster growth

508 Acidification, warming, and nutrient reductions are projected to affect shell and tissue growth of oysters in different  
509 ways. Here, increased atmospheric CO<sub>2</sub> caused reductions in shell growth of Eastern oysters due to its negative effect on  $\Omega_{Ca}$   
510 and thus calcification rates, which is consistent with experimental studies (Waldbusser et al., 2011; Gobler and Talmage, 2014;  
511 Himes et al., 2024). Shell weight reductions from increased atmospheric CO<sub>2</sub> were driven by changes in calcification rate  
512 alone, as tissue weight in *EcoOyster* is unaffected by  $\Omega_{Ca}$  (Fig. 11d; Rivest et al., 2023). Experimental studies have identified  
513 indirect physiological impacts of elevated CO<sub>2</sub> on juvenile/adult oyster metabolism, growth, and reproduction (Beniash et al.,  
514 2010; Dickinson et al., 2012), suggesting that increased atmospheric CO<sub>2</sub> can sometimes influence tissue growth. Further  
515 investigation is necessary in order to include the relationship between atmospheric CO<sub>2</sub> and oyster tissue growth in *EcoOyster*.  
516 Biological and chemical reactions occur faster at higher temperatures, meaning calcification rates may be higher under future  
517 warming conditions (Waldbusser et al., 2011), as long as  $\Omega_{Ca}$  is still high enough to support calcification. Conversely, under  
518 conditions of extreme low  $\Omega_{Ca}$ , warming may exacerbate dissolution rates and shell weight reductions. Our results also show  
519 that nutrient reductions will lead to reductions in shell weight, largely driven by a reduction in tissue weight resulting from  
520 lower food availability (POC), rather than lower  $\Omega_{Ca}$ .

521 While nutrient reductions are projected to have little influence on  $\Omega_{Ca}$  in this study, their negative influence on food  
522 availability may be detrimental to tissue growth in certain parts of the study region, particularly the York River. Our model  
523 projections suggest that nutrient reductions may in some cases produce conditions that do not support any oyster growth along  
524 the shoals of the York (Fig. 9c; 10c), a result of reductions in food availability that are predicted to be more substantial in the  
525 tributaries than the mainstem region (Fig. 6c). Multiple studies have demonstrated that Eastern oysters and other calcifying  
526 organisms perform better under acidification when they have sufficient food availability, as they are better able to keep up  
527 with the energetic demands of environmental stress (Thomsen et al., 2015; Ramajo et al., 2016; Schwaner et al., 2023).  
528 Therefore, nutrient reductions will likely influence oyster growth under acidification stress by different magnitudes in each  
529 tributary. When comparing the effects of local management actions to reduce nutrient runoff to the effects of climate change  
530 (increased atmospheric CO<sub>2</sub> and warming), it is evident that, on average, climate change will have a much greater negative  
531 influence on oyster growth (Table 4). However, the strong localized impacts of nutrient reductions in the York highlight the



532 importance of examining the spatial variability of future changes in oyster growth. It is important for managers to consider  
533 local conditions when assessing the effects of nutrient reductions on oyster production.

534 Increased water temperatures are projected to slow oyster growth in the future. Specifically, large reductions in tissue  
535 weight are underpinned by three primary mechanisms: limitations on filtration at high temperatures (Loosanoff, 1958),  
536 increased respiration rates (Dame, 1972), and reduced food availability. In *EcoOyster*, the optimal temperature for Eastern  
537 oyster filtration is 27°C (Cerco et al., 2005; Jordan, 1987), and under warming, the frequency at which ambient summer  
538 temperatures will surpass this optimal temperature will be higher (Fig. 7a), therefore causing more frequent declines in  
539 filtration rate (Cerco et al., 2005; Fulford et al., 2007). There is no clear optimal temperature for oyster respiration, and  
540 therefore it is assumed to increase exponentially with temperature (Hochachka and Somero, 2002). Thus, as oyster filtration  
541 rates begin to decline at high temperatures, respiration rates will continue to rise and decrease the potential for tissue  
542 accumulation (Fig. S1). Previous studies on juvenile Eastern oysters do not support a consensus on the relationship between  
543 warming and tissue growth. Some report that growth is inhibited at higher temperatures (31°C, Stevens and Gobler, 2018;  
544 30°C, Speights et al., 2017). In contrast, Talmage and Gobler (2011) found no significant influence of high temperature (28°C)  
545 alone on tissue growth. The optimal temperature for oyster filtration may also vary among oysters, based on observations of  
546 maximum filtration rates of adult Eastern oysters occurring between 28.1°C– 32°C (Loosanoff, 1958). Variation in  
547 experimental design may have contributed to the contrast in results summarized here, in addition to the influence of local  
548 adaptation (Burford et al., 2014). Other studies that incorporate higher temperature thresholds into their models predict  
549 increases in oyster biomass under warming in Chesapeake Bay (Allen et al., 2023), underscoring the importance of properly  
550 parameterizing growth models. Due to a lack of consensus on temperature limits of Eastern oyster filtration, further research  
551 is needed to more robustly represent oyster filtration in bioenergetics models and improve predictions of impacts of warming  
552 on oysters and their ecosystem services in the region.

553 Warming will likely have a negative effect on food availability for oysters. Compared to the effects of nutrient  
554 reductions, warming will have a much more widespread influence on POC, causing reductions throughout the model domain  
555 (Fig. 10b,c). Despite warming increasing rates of POC production via increased phytoplankton growth rates, factors such as  
556 nutrient limitation and increased respiration rates will result in a net decrease in POC availability. In the tributaries, reductions  
557 in food availability will be most widespread due to warming, but less extreme than those from nutrient reductions in the shallow  
558 parts of the tributaries where oysters are affected. Remineralization of organic carbon in marine systems is temperature-  
559 dependent (López-Urrutia et al., 2006), and as warming occurs, remineralization of detrital carbon to DIC in bottom waters  
560 will occur at higher rates. As much of the lower bay is nutrient-limited (Zhang et al., 2021), phytoplankton growth rates will  
561 not increase much from warming alone; therefore, increased remineralization will likely reduce the overall amount of food  
562 available to oysters. Despite a similar average reduction in food availability being predicted for the future warming simulation  
563 and managed nutrient reductions simulation, the influence of warmer temperatures will amplify the negative effects of reduced  
564 food availability on growth. In this study, the critical temperature at which respiration rates exceed assimilation rates is  
565 dependent on filtration. When food availability limits filtration, this critical temperature lowers, and the temperature threshold



566 for tissue loss is lowered. Experimental studies have demonstrated how organic carbon may be influenced by both warming  
567 and acidification (Simone et al., 2021), but as these dynamics can differ based on nutrient availability, it is important to consider  
568 how climate change will influence food webs and nutrient dynamics.

569 The projected mid-century reductions in oyster growth obtained from this analysis are consistent with the results of  
570 other studies that examine oyster growth under projected climate change conditions. A study modeling oyster responses in  
571 Barataria Bay, LA, for example, predicts that under a warming and high flow scenario (though without the effects of future  
572 nutrient reductions or atmospheric CO<sub>2</sub>), oysters will experience widespread mortality in fresher parts of the bay by the end of  
573 the century (Lavaud et al., 2021). Experimental studies have shown similar negative effects of acidification, warming, lower  
574 food availability, and increased freshwater flow on oyster survival (La Peyre et al., 2013; Rybovich et al., 2016; Lowe et al.,  
575 2019; Jones et al., 2019). Da (2023) found that the reductions in salinity and  $\Omega_{Ca}$  that result from high discharge events in the  
576 York River will increase in extent as climate change progresses and increasingly threaten aquaculture production. In the  
577 Chesapeake Bay, extreme precipitation events are predicted to occur more frequently with future climate change, however an  
578 overall decline in annual average precipitation is also predicted (St. Laurent et al., 2021). As a result, the overall impact of  
579 freshwater from the land is not projected to change significantly in the future (Hinson et al., 2023). Changes in precipitation  
580 were thus not simulated in this study, but future work could examine the dynamics of climate change, salinity,  $\Omega_{Ca}$ , and oyster  
581 growth in a year with more heavy rainfall events but lower annual rainfall.

### 582 **4.3 Influence of future changes in oyster growth on aquaculture**

583 Understanding the relative impacts of global climate change and local nutrient management actions on oyster growth  
584 and survival will allow aquaculture producers to anticipate how their oyster stock may respond to these anthropogenic changes.  
585 As the effects of climate change are subject to natural interannual variability, the magnitude of acidification and warming in a  
586 given year will likely differ (Cai et al., 2021; Moore-Maley et al., 2016; Li et al., 2016), influencing oyster growth through  
587 differing mechanisms. Smaller oysters resulting from slower growing times in a particularly warm year may present a different  
588 challenge to growers than weak-shelled oysters in a year with lower  $\Omega_{Ca}$  and average temperatures. Mortality may also become  
589 a more urgent challenge as summer temperatures warm. A previous study examining commercial performance of Pacific  
590 oysters in Brazil found that interannual variability in temperature, *chl a* abundance, and climate events influenced survival and  
591 growth phase timing (Mizuta et al., 2012). High temperatures inhibited survival of oyster seed in that study, which frequently  
592 occurs in Pacific oysters (*Crassostrea gigas*) during the summer months in Europe and California (Gouletquer et al., 1998;  
593 Burge et al., 2007; Malhan et al., 2009). A similar phenomenon has been observed in Eastern oysters; however, mortality  
594 events in this species have not been conclusively linked to warmer water temperatures (Guevelou et al., 2019; Biranik and  
595 Allam, 2023), and the cause is yet to be resolved for either species. Nonetheless, the increasing occurrence of spring/summer  
596 mortality in Eastern oysters suggests that shifting the time of planting oysters on leases later in the year may help mitigate the  
597 risk of widespread mortality, although the economic tradeoffs involved in shifting the growing season for oysters should be  
598 taken into account.



599 Future climate change and nutrient management are projected to worsen conditions for oyster growth, and the spatial  
600 variation in these changes may unevenly influence aquaculture production. While reductions in shell and tissue growth are  
601 predicted for nearly all regions where oysters grow, these changes will likely differ based on present-day environmental  
602 conditions. Under present day conditions, the most oyster growth is projected to occur in regions with some of the highest  
603 present-day  $\Omega_{Ca}$  and the greatest projected  $\Omega_{Ca}$  reductions, i.e., in the Rappahannock River and mainstem shoals. Some of the  
604 most dramatic tissue and shell reductions are projected to occur in the York and upper Rappahannock, where reduced food  
605 availability and low  $\Omega_{Ca}$  will limit oyster filtration and shell growth. Oysters in parts of both the Rappahannock and York  
606 Rivers will likely face mortality (represented by near complete depletion of oyster shell and tissue) by mid-century (Figs. 8,  
607 9). However, these reductions will not be spatially uniform, underscoring the importance of oyster farm site selection within a  
608 tributary. In contrast, oysters grown outside the tributaries are projected to exhibit a smaller decline in growth, indicating  
609 greater future opportunity for oyster farming in these locations. Under the business-as-usual climate change trajectory analyzed  
610 here, bottom conditions in the tributaries will be less suitable for oyster aquaculture by mid-century, and producers might  
611 consider alternate farm locations or shifting production methods toward floating culture to avoid exposure to low  $\Omega_{Ca}$   
612 conditions and access greater food availability.

613 Beyond reduced oyster growth, aquaculture operations may also be affected in the future by temporal changes in  
614 optimal growing conditions. Due to the input of freshwater that lowers DIC and TA and increases  $pCO_2$  (Cai et al., 2017; Cai  
615 et al., 2021; Da et al., 2024), the greatest magnitude of  $\Omega_{Ca}$  reductions occurs in spring. The majority of oyster growth is  
616 projected to occur in the spring and summer (Fig. 7), so changes to growing conditions may be most consequential during  
617 these warmer months. Deployment of oyster seed generally begins in the spring and continues into the summer, so it is  
618 important for producers to be aware of ambient conditions being experienced by their newly deployed oysters. As spring  
619 temperatures warm, phytoplankton blooms will likely occur earlier in the year, shifting the time when food availability is  
620 highest (Da et al., 2021). Oysters deployed earlier in the year may benefit from greater food availability and perform better  
621 than oysters deployed in July or August when waters are warmest. However, they may also face the challenge of spring/summer  
622 mortality events, revealing the complexity of timing oyster deployment under worsening climate change conditions. For oyster  
623 farms closer to freshwater sources, the combined effects of low  $\Omega_{Ca}$ , low salinity, and high summer temperatures may severely  
624 inhibit growth and extend time-to-market.

#### 625 4.4 Future work

626 Providing the aquaculture industry with the best existing estimates of climate change impacts to their operations will  
627 allow them to make more informed decisions about their future practices. This study used a 120-meter horizontal resolution  
628 model grid to examine near-lease-level effects of climate change and management actions on oyster growth in a section of the  
629 lower Chesapeake Bay. Similar studies with high resolution model grids in other systems will strengthen our understanding of  
630 how regional anthropogenic effects will influence the oyster aquaculture sector and could be used to identify areas of  
631 opportunity for new aquaculture practices (Swam et al., 2022; Palmer et al., 2021; Lavaud et al., 2024). The present study



632 incorporated one Earth System Model and one emissions scenario; future work should quantify how these choices impact  
633 estimates of future  $\Omega_{Ca}$  and oyster growth (e.g., Hinson et al., 2023). Future modeling studies should also incorporate other  
634 climate change impacts, such as sea level rise and increased storminess which are projected to influence conditions for oyster  
635 growth in the Chesapeake Bay region (Seneviratne et al., 2012; Lowe et al., 2019, Rybovich et al., 2016, Jones et al., 2019).

636 To improve estimates of shell and tissue growth of oysters under climate change, additional experimental studies  
637 should be conducted to reduce the data gaps that currently limit model formulations. Uncertainties in the functional  
638 relationships and rate parameters used in these models may lead to an inaccurate influence of some environmental variables  
639 on oyster growth. For example, results in this study may be particularly sensitive to the optimum temperature for filtration  
640 rate. Reductions in tissue weight are particularly dramatic when average temperature conditions at oyster lease sites remain  
641 above this optimal temperature from mid-June through late August, a vital time for oyster growth. As a result, growth in the  
642 model is sensitive to the simulation start date, and future studies should compare the influence of warming on growth in  
643 simulations that start at different times in the year. Many physiological studies of temperature impacts on oyster filtration date  
644 back to the mid-to-late-20<sup>th</sup> century, and present-day seasonal extremes that coastal organisms experience may routinely exceed  
645 the maximum temperatures used in many of these earlier experimental designs. For example, Jordan (1987) used a maximum  
646 temperature of 27 °C, which was the ambient temperature when samples were collected in July from the Choptank River, MD.  
647 Between 1985 and 2014, bottom waters of the north mesohaline Bay main stem (closest to the Choptank) warmed  $1.01 \pm 0.13$   
648 °C during May to October (Hinson et al., 2022), and the present study predicts a  $1.5 \pm 0.26$  °C increase across the entire model  
649 domain between 2017 and mid-century. To build stronger models of future climate impacts, and to expand scientific  
650 understanding of physiological limits of the Eastern oyster, future studies should re-examine temperature limitations on oyster  
651 filtration and respiration by using higher experimental temperatures.

652 As oyster growth is highly sensitive to food availability, improved measurements of particulate organic carbon in the  
653 region would fortify projections of oyster production under future climate change and nutrient management. Here, it is assumed  
654 that oysters feed on POC, a combination of plankton and detritus. However, average POC concentrations are highly  
655 spatiotemporally variable in the Chesapeake Bay due to eutrophication and algal blooms. In this study, POC was  
656 underestimated in the tributary channels; however, it is unclear how well POC was estimated in oyster growing areas, as *in*  
657 *situ* measurements are currently limited to stations in the channels during monthly or semi-monthly sampling cruises. More  
658 routine POC measurements, as well as measurements of POC in regions where oyster farming operations occur, are needed to  
659 verify the spatiotemporal dynamics of food availability. Improved measurements of oyster food availability would allow for  
660 stronger model skill assessment and improved projections of oyster production.

## 661 5 Conclusions

662 This study predicts widespread reductions in  $\Omega_{Ca}$  in the lower Virginia tributaries of the Chesapeake Bay by mid-  
663 century, highlighting the use of high-resolution model projections to better understand present-day carbonate chemistry  
664 conditions and to predict the effects of climate change on a region of high interest for aquaculture production. While similar



665 modeling studies have projected acidification conditions in coastal regions with 3D coupled models (Siedlecki et al., 2021a,b;  
666 Fujii et al., 2023) or modeled oyster growth with remote-sensing data and dynamic energy budget models (Palmer et al., 2020;  
667 Palmer et al., 2021; Bertollini et al., 2021), the present study projects both carbonate chemistry conditions and oyster  
668 bioenergetics in the Chesapeake Bay with the highest resolution thus far. Specifically, widespread reductions in  $\Omega_{Ca}$  will  
669 negatively impact oyster growth, with implications for aquaculture operations and local and regional economies. As bottom  
670 conditions worsen, altered site-selection for oyster farms or other adaptive measures will become imperative to sustain  
671 production and reduce the impacts of low  $\Omega_{Ca}$  on farmed oysters.

672 Increased atmospheric  $CO_2$  and nutrient reductions are projected to inhibit oyster calcification, while warming and  
673 nutrient reductions will reduce oyster tissue and shell growth due to limitations on filtration and lowered food availability.  
674 While the effects of global climate change on oyster growth are projected to be much stronger overall than the effects of local  
675 nutrient management, lowered food availability from nutrient reductions may have a strong influence on oyster growth in  
676 certain parts of the study region. As a result, all areas will not be equally vulnerable to future changes in the atmosphere and  
677 watershed. Understanding how individual drivers influence oyster growth is important for predicting effects on aquaculture  
678 production in the context of interannual variability of climate change and nutrient management outcomes. While the negative  
679 effects of temperature on growth were strong in this study, additional studies on Eastern oyster temperature limits are needed  
680 to improve projections, particularly as summer mortality of oysters is already common. Increased *in situ* measurements of  
681 biogeochemical variables and experimental studies on oyster physiology and bioenergetics will allow for improved projections  
682 of mid-century conditions and their potential impacts on oyster growth and the aquaculture industry.

683

#### 684 **Code Availability**

685 Model code will be available upon request.

686

#### 687 **Data Availability**

688 Model output will be available with a DOI on William & Mary ScholarWorks.

689

#### 690 **Author Contribution**

691 MAMF, EBR, MJB, and PS wrote the proposal and acquired the funding for the project; MAMF, PS, and FD developed the  
692 ROMS-ECB code; MJB developed the EcoOyster code; CC, MAMF, and EBR designed the experiment; CC ran model  
693 simulations, analyzed the output, created the figures, and wrote the manuscript draft; MAMF, EBR, MJB, PS, and FD reviewed  
694 and edited the manuscript.

695

#### 696 **Competing Interests**

697 The authors declare that they have no conflict of interest.

698



699 **Acknowledgements**

700 This paper is the result of research funded by the National Oceanic and Atmospheric Administration's Ocean Acidification  
701 Program under award NA18OAR0170430 to the Virginia Institute of Marine Science (VIMS). We would like to thank the  
702 VIMS and William & Mary (W&M) high performance computing group for their technical support and computing resources.  
703 We also thank the NOAA Chesapeake Bay Program for providing us with watershed inputs from their Phase 6 Watershed  
704 Model. This work was largely made possible by Sara Blachman's hard work on the EcoOyster model. We thank Bill Walton  
705 for his aquaculture expertise and support throughout the project. The model results used for this manuscript are available at  
706 W&M Scholarworks.

707 **References**

- 708 Abatzoglou, J. T. and Brown, T. J.: A comparison of statistical downscaling methods suited for wildfire applications, *Int. J.*  
709 *Clim.*, 32, 772–780, <https://doi.org/10.1002/joc.2312>, 2012.
- 710 Allen, K. L., Ihde, T., Knoche, S., Townsend, H., & Lewis, K. A.: Simulated climate change impacts on striped bass, blue crab  
711 and Eastern oyster in oyster sanctuary habitats of Chesapeake Bay. *Estuar. Coast. Shelf Sci.*, 292, 108465,  
712 <https://doi.org/10.1016/j.ecss.2023.108465>, 2023.
- 713 Amaral, V., Cabral, H. N., and Bishop, M. J.: Effects of estuarine acidification on predator–prey interactions. *Mar. Eco. Prog.*  
714 *Ser.*, 445, 117-127, <https://doi.org/10.3354/meps09487>, 2012.
- 715 Barclay, K.M., Gingras, M.K., Packer, S.T. and Leighton, L.R.: The role of gastropod shell composition and microstructure in  
716 resisting dissolution caused by ocean acidification, *Mar. Environ. Res.*, 162, 105105,  
717 <https://doi.org/10.1016/j.marenvres.2020.105105>, 2020.
- 718 Barton, S. and Yvon-Durocher, G.: Quantifying the temperature dependence of growth rate in marine phytoplankton within  
719 and across species, *Limnol. Oceanogr.*, 64, 2081–2091, <https://doi.org/10.1002/lno.11170>, 2019.
- 720 Beniash, E., Ivanina, A., Lieb, N., Kurochkin, I., and Sokolova, I.: Elevated level of carbon dioxide affects metabolism and  
721 shell formation in oysters *Crassostrea virginica* (Gmelin), *Mar. Ecol. Prog. Ser.*, 419, 95–108,  
722 <https://doi.org/10.3354/meps08841>, 2010.
- 723 Bertolini, C., Brigolin, D., Porporato, E. M. D., Hattab, J., Pastres, R., and Tiscar, P. G.: Testing a Model of Pacific Oysters'  
724 (*Crassostrea gigas*) Growth in the Adriatic Sea: Implications for Aquaculture Spatial Planning, *Sustainability*, 13, 3309,  
725 <https://doi.org/10.3390/su13063309>, 2021.
- 726 Bhatt, G., Linker, L., Shenk, G., Bertani, I., Tian, R., Rigelman, J., Hinson, K., and Claggett, P.: Water quality impacts of  
727 climate change, land use, and population growth in the Chesapeake Bay watershed, *JAWRA J. Am. Water Resour. Assoc.*, 59,  
728 1313–1341, <https://doi.org/10.1111/1752-1688.13144>, 2023.
- 729 Borges, A. V. and Gypens, N.: Carbonate chemistry in the coastal zone responds more strongly to eutrophication than to ocean  
730 acidification, *Limnol. Oceanogr.*, 55, 346–353, <https://doi.org/10.4319/lo.2010.55.1.0346>, 2010.





- 731 Boulais, M., Chenevert, K. J., Demey, A. T., Darrow, E. S., Robison, M. R., Roberts, J. P., and Volety, A.: Oyster reproduction  
732 is compromised by acidification experienced seasonally in coastal regions, *Sci. Rep.*, 7, 13276, [https://doi.org/10.1038/s41598-](https://doi.org/10.1038/s41598-017-13480-3)  
733 017-13480-3, 2017.
- 734 Brianik, C. J. and Allam, B.: The need for more information on the resistance to biological and environmental stressors in  
735 triploid oysters, *Aquaculture*, 577, 739913, <https://doi.org/10.1016/j.aquaculture.2023.739913>, 2023.
- 736 Bukaveckas, P. A.: Carbon dynamics at the river–estuarine transition: a comparison among tributaries of Chesapeake Bay,  
737 *Biogeosciences*, 19, 4209–4226, <https://doi.org/10.5194/bg-19-4209-2022>, 2022.
- 738 Brush, M.J., and M.L. Kellogg: Harris Creek Oyster Restoration Model v2. Virginia Institute of Marine Science, Gloucester  
739 Point, VA, <https://www.vims.edu/research/departments/bio/programs/sempr/models/index.php>, 2018.
- 740 Burford, M., Scarpa, J., Cook, B., and Hare, M.: Local adaptation of a marine invertebrate with a high dispersal potential:  
741 evidence from a reciprocal transplant experiment of the eastern oyster *Crassostrea virginica*, *Mar. Ecol. Prog. Ser.*, 505, 161–  
742 175, <https://doi.org/10.3354/meps10796>, 2014.
- 743 Burge, C. A., Judah, L. R., Conquest, L. L., Griffin, F. J., Cheney, D. P., Suhrbier, A., Vadopalas, B., Olin, P. G., Renault, T.,  
744 and Friedman, C. S.: Summer seed mortality of the pacific oyster, *Crassostrea gigas* (Thunberg) grown in Tomales Bay,  
745 California, USA: the influence of oyster stock, planting time, pathogens, and environmental stressors, *J. Shellfish Res.*,  
746 <https://doi.org/10.2983/0730-8000>, 2007.
- 747 Cai, W., Feely, R. A., Testa, J. M., Li, M., Evans, W., Alin, S. R., Xu, Y.-Y., Pelletier, G., Ahmed, A., Greeley, D. J., Newton,  
748 J. A., and Bednaršek, N.: Natural and Anthropogenic Drivers of Acidification in Large Estuaries, *Annu. Rev. Mar. Sci.*,  
749 <https://doi.org/10.1146/annurev-marine-010419-011004>, 2021.
- 750 Cai, W.J., Huang, W.-J., Luther, G. W., Pierrot, D., Li, M., Testa, J., Xue, M., Joesoef, A., Mann, R., Brodeur, J., Xu, Y.-Y.,  
751 Chen, B., Hussain, N., Waldbusser, G. G., Cornwell, J., and Kemp, W. M.: Redox reactions and weak buffering capacity lead  
752 to acidification in the Chesapeake Bay, *Nat. Commun.*, 8, 369, <https://doi.org/10.1038/s41467-017-00417-7>, 2017.
- 753 Cai, W.J., Xu, Y.-Y., Feely, R. A., Wanninkhof, R., Jönsson, B., Alin, S. R., Barbero, L., Cross, J. N., Azetsu-Scott, K.,  
754 Fassbender, A. J., Carter, B. R., Jiang, L.-Q., Pepin, P., Chen, B., Hussain, N., Reimer, J. J., Xue, L., Salisbury, J. E.,  
755 Hernández-Ayón, J. M., Langdon, C., Li, Q., Sutton, A. J., Chen, C.-T. A., and Gledhill, D. K.: Controls on surface water  
756 carbonate chemistry along North American ocean margins, *Nat. Commun.*, 11, 2691, [https://doi.org/10.1038/s41467-020-](https://doi.org/10.1038/s41467-020-16530-z)  
757 16530-z, 2020.
- 758 Cai, W. J., and Wang, Y.: The chemistry, fluxes, and sources of carbon dioxide in the estuarine waters of the Satilla and  
759 Altamaha Rivers, Georgia. *Limnol. Oceanogr.*, 43(4), 657-668, <https://doi.org/10.4319/lo.1998.43.4.0657>, 1998.
- 760 Caldeira, K. and Wickett, M. E.: Anthropogenic carbon and ocean pH, *Nature*, 425, 365–365, <https://doi.org/10.1038/425365a>,  
761 2003.
- 762 Caldeira, K. and Wickett, M. E.: Ocean model predictions of chemistry changes from carbon dioxide emissions to the  
763 atmosphere and ocean, *J. Geophys. Res.: Oceans*, 110, <https://doi.org/10.1029/2004jc002671>, 2005.



- 764 Callam, B. R., Allen, S. K., and Frank-Lawale, A.: Genetic and environmental influence on triploid *Crassostrea virginica*  
765 grown in Chesapeake Bay: Growth, Aquaculture, 452, 97–106, <https://doi.org/10.1016/j.aquaculture.2015.10.027>, 2016.
- 766 Carstensen, J. and Duarte, C. M.: Drivers of pH Variability in Coastal Ecosystems, Environ. Sci. Technol., 53, 4020–4029,  
767 <https://doi.org/10.1021/acs.est.8b03655>, 2019.
- 768 Cerco, C. and Noel, M.: Process-based primary production modeling in Chesapeake Bay, Mar. Ecol. Prog. Ser., 282, 45–58,  
769 <https://doi.org/10.3354/meps282045>, 2004.
- 770 Cerco, C. F. and Noel, M. R.: Nonnative Oysters in the Chesapeake Bay, 2005.
- 771 Cerco, C. F., Noel, M. R., and Wang, P.: The Shallow-Water Component of the Chesapeake Bay Environmental Model  
772 Package, JAWRA J. Am. Water Resour. Assoc., 49, 1091–1102, <https://doi.org/10.1111/jawr.12106>, 2013.
- 773 Chesapeake Bay Program DataHub: <https://datahub.chesapeakebay.net/>, last access: 28 January 2024
- 774 Comeau, L. A., Mayrand, É., and Mallet, A.: Winter quiescence and spring awakening of the Eastern oyster *Crassostrea*  
775 *virginica* at its northernmost distribution limit, Mar. Biol., 159, 2269–2279, <https://doi.org/10.1007/s00227-012-2012-8>, 2012.
- 776 Copernicus Climate Change Service: ERA5: Fifth Generation of ECMWF Atmospheric Reanalyses of the Global Climate,  
777 Copernicus Climate Change Service Climate Data Store (CDS). <https://cds.climate.copernicus.eu/cdsapp#!/home>, 2017.
- 778 Da, F., Friedrichs, M. A. M., St-Laurent, P., Shadwick, E. H., Najjar, R. G., and Hinson, K. E.: Mechanisms Driving Decadal  
779 Changes in the Carbonate System of a Coastal Plain Estuary, J. Geophys. Res.: Oceans, 126,  
780 <https://doi.org/10.1029/2021jc017239>, 2021.
- 781 Da, F.: Chesapeake Bay Carbon Cycle: Past, Present, Future, PhD. Dissertation, Virginia Institute of Marine Science, William  
782 & Mary, Virginia, USA, <https://dx.doi.org/10.25773/v5-46f7-e286>, 2023.
- 783 Da, F., Friedrichs, M. A. M., St-Laurent, P., Najjar, R. G., Shadwick, E. H., and Stets, E. G.: Influence of Rivers, Tides, and  
784 Tidal Wetlands on Estuarine Carbonate System Dynamics, Estuaries Coasts, 1-23, [https://doi.org/10.1007/s12237-024-01421-](https://doi.org/10.1007/s12237-024-01421-z)  
785 *z*, 2024.
- 786 Dame, R.F.: The ecological energies of growth, respiration and assimilation in the intertidal American oyster *Crassostrea*  
787 *virginica*, Mar. Biol., 17, 43-250, 1972.
- 788 Dayton, P.K.: Toward an understanding of community resilience and the potential effects of enrichments to the benthos at  
789 McMurdo Sound, Antarctica, Proceedings of the colloquium on conservation problems in Antarctica, 81-96, 1972.
- 790 Dégremont, L., Garcia, C., Frank-Lawale, A., and Allen, S. K.: Triploid Oysters in the Chesapeake Bay: Comparison of Diploid  
791 and Triploid *Crassostrea virginica*, J. Shellfish Res., 31, 21–31, <https://doi.org/10.2983/035.031.0103>, 2012.
- 792 Dickinson, G. H., Ivanina, A. V., Matoo, O. B., Pörtner, H. O., Lannig, G., Bock, C., Beniash, E., and Sokolova, I. M.:  
793 Interactive effects of salinity and elevated CO<sub>2</sub> levels on juvenile eastern oysters, *Crassostrea virginica*, J. Exp. Biol., 215, 29–  
794 43, <https://doi.org/10.1242/jeb.061481>, 2011.
- 795 Dinauer, A. and Mucci, A.: Spatial variability in surface-water pCO<sub>2</sub> and gas exchange in the world's largest semi-enclosed  
796 estuarine system: St. Lawrence Estuary (Canada), Biogeosciences, 14, 3221-3237, <https://doi.org/10.5194/bg-14-3221-2017>,  
797 2017.



- 798 Doney, S. C., Fabry, V. J., Feely, R. A., and Kleypas, J. A.: Ocean acidification: the other CO<sub>2</sub> problem., *Annu. Rev. Mar.*  
799 *Sci.*, 1, 169–92, <https://doi.org/10.1146/annurev.marine.010908.163834>, 2009.
- 800 Dong, S., Lei, Y., Li, T., Cao, Y., and Xu, K.: Biocalcification crisis in the continental shelf under ocean acidification. *Geosci.*  
801 *Front.*, 14(6), 101622, <https://doi.org/10.1016/j.gsf.2023.101622>, 2023.
- 802 Du, J., Shen, J., Park, K., Wang, Y. P., and Yu, X.: Worsened physical condition due to climate change contributes to the  
803 increasing hypoxia in Chesapeake Bay, *Sci. Total Environ.*, 630, 707–717, <https://doi.org/10.1016/j.scitotenv.2018.02.265>,  
804 2018.
- 805 Duarte, C. M., Hendriks, I. E., Moore, T. S., Olsen, Y. S., Steckbauer, A., Ramajo, L., Carstensen, J., Trotter, J. A., and  
806 McCulloch, M.: Is Ocean Acidification an Open-Ocean Syndrome? Understanding Anthropogenic Impacts on Seawater pH,  
807 *Estuaries Coasts*, 36, 221–236, <https://doi.org/10.1007/s12237-013-9594-3>, 2013.
- 808 Dufresne, J.-L., Foujols, M.-A., Denvil, S., Caubel, A., Marti, O., Aumont, O., Balkanski, Y., Bekki, S., Bellenger, H.,  
809 Benschila, R., Bony, S., Bopp, L., Braconnot, P., Brockmann, P., Cadule, P., Cheruy, F., Codron, F., Cozic, A., Cugnet, D.,  
810 Noblet, N. de, Duvel, J.-P., Ethé, C., Fairhead, L., Fichet, T., Flavoni, S., Friedlingstein, P., Grandpeix, J.-Y., Guez, L.,  
811 Guilyardi, E., Hauglustaine, D., Hourdin, F., Idelkadi, A., Ghattas, J., Joussaume, S., Kageyama, M., Krinner, G., Labetoulle,  
812 S., Lahellec, A., Lefebvre, M.-P., Lefevre, F., Levy, C., Li, Z. X., Lloyd, J., Lott, F., Madec, G., Mancip, M., Marchand, M.,  
813 Masson, S., Meurdesoif, Y., Mignot, J., Musat, I., Parouty, S., Polcher, J., Rio, C., Schulz, M., Swingedouw, D., Szopa, S.,  
814 Talandier, C., Terray, P., Viovy, N., and Vuichard, N.: Climate change projections using the IPSL-CM5 Earth System Model:  
815 from CMIP3 to CMIP5, *Clim. Dyn.*, 40, 2123–2165, <https://doi.org/10.1007/s00382-012-1636-1>, 2013.
- 816 Dunne, J. P., John, J. G., Adcroft, A. J., Griffies, S. M., Hallberg, R. W., Shevliakova, E., Stouffer, R. J., Cooke, W., Dunne,  
817 K. A., Harrison, M. J., Krasting, J. P., Malyshev, S. L., Milly, P. C. D., Phillipps, P. J., Sentman, L. T., Samuels, B. L., Spelman,  
818 M. J., Winton, M., Wittenberg, A. T., and Zadeh, N.: GFDL’s ESM2 Global Coupled Climate–Carbon Earth System Models.  
819 Part I: Physical Formulation and Baseline Simulation Characteristics, *J. Clim.*, 25, 6646–6665, <https://doi.org/10.1175/jcli-d->  
820 [11-00560.1](https://doi.org/10.1175/jcli-d-11-00560.1), 2012.
- 821 EPA, Chesapeake Bay Total Maximum Daily Load for Nitrogen, Phosphorus, and Sediment, United States Environmental  
822 Protection Agency, 2010.
- 823 Guinotte, J. M. and Fabry, V. J.: Ocean Acidification and Its Potential Effects on Marine Ecosystems, *Ann. N. York Acad.*  
824 *Sci.*, 1134, 320–342, <https://doi.org/10.1196/annals.1439.013>, 2008.
- 825 Ehrlich, M. K. and Harris, L. A.: A review of existing eastern oyster filtration rate models, *Ecol. Model.*, 297, 201–212,  
826 <https://doi.org/10.1016/j.ecolmodel.2014.11.023>, 2015.
- 827 Feely, R. A., Sabine, C. L., Lee, K., Berelson, W., Kleypas, J., Fabry, V. J., and Millero, F. J.: Impact of Anthropogenic CO<sub>2</sub>  
828 on the CaCO<sub>3</sub> System in the Oceans, *Science*, 305, 362–366, <https://doi.org/10.1126/science.1097329>, 2004.
- 829 Feely, R. A., Doney, S. C., and Cooley, S. R.: Ocean Acidification: Present Conditions and Future Changes in a High-CO<sub>2</sub>  
830 World, *Oceanography*, 22, 36–47, <https://doi.org/10.5670/oceanog.2009.95>, 2009.



- 831 Feng, Y., Friedrichs, M. A. M., Wilkin, J., Tian, H., Yang, Q., Hofmann, E. E., Wiggert, J. D., and Hood, R. R.: Chesapeake  
832 Bay nitrogen fluxes derived from a land-estuarine ocean biogeochemical modeling system: Model description, evaluation, and  
833 nitrogen budgets, *J. Geophys. Res.: Biogeosciences*, 120, 1666–1695, <https://doi.org/10.1002/2015jg002931>, 2015.
- 834 Fitzer, S. C., Torres Gabarda, S., Daly, L., Hughes, B., Dove, M., O'Connor, W., Potts, J., Scanes, P., and Byrne, M.: Coastal  
835 acidification impacts on shell mineral structure of bivalve mollusks. *Ecol. Evol.*, 8(17), 8973–8984,  
836 <https://doi.org/10.1002/ece3.4416>, 2018.
- 837 Frankel, L. T., Friedrichs, M. A. M., St-Laurent, P., Bever, A. J., Lipcius, R. N., Bhatt, G., and Shenk, G. W.: Nitrogen  
838 reductions have decreased hypoxia in the Chesapeake Bay: Evidence from empirical and numerical modeling, *Sci. Total  
839 Environ.*, 814, 152722, <https://doi.org/10.1016/j.scitotenv.2021.152722>, 2022.
- 840 Frank-Lawale, A., Allen, S. K., and Dgremont, L.: Breeding and Domestication of Eastern Oyster (*Crassostrea virginica*) Lines  
841 for Culture in the Mid-Atlantic, Usa: Line Development and Mass Selection for Disease Resistance, *J. Shellfish Res.*, 33, 153–  
842 165, <https://doi.org/10.2983/035.033.0115>, 2014.
- 843 Fujii, M., Hamanoue, R., Bernardo, L. P. C., Ono, T., Dazai, A., Oomoto, S., Wakita, M., and Tanaka, T.: Assessing impacts  
844 of coastal warming, acidification, and deoxygenation on Pacific oyster (*Crassostrea gigas*) farming: a case study in the Hinase  
845 area, Okayama Prefecture, and Shizugawa Bay, Miyagi Prefecture, Japan, *Biogeosciences*, 20, 4527–4549,  
846 <https://doi.org/10.5194/bg-20-4527-2023>, 2023.
- 847 Fulford, R., Breitburg, D., Newell, R., Kemp, W., and Luckenbach, M.: Effects of oyster population restoration strategies on  
848 phytoplankton biomass in Chesapeake Bay: a flexible modeling approach, *Mar. Ecol. Prog. Ser.*, 336, 43–61,  
849 <https://doi.org/10.3354/meps336043>, 2007.
- 850 Gattuso, Strong, A. L., Kroeker, K. J., Teneva, L. T., Mease, L. A., and Kelly, R. P.: Ocean Acidification 2.0: Managing our  
851 Changing Coastal Ocean Chemistry, *BioScience*, 64, 581–592, <https://doi.org/10.1093/biosci/biu072>, 2014.
- 852 Gawde, R. K., North, E. W., Hood, R. R., Long, W., Wang, H., and Wilberg, M. J.: A high resolution hydrodynamic-  
853 biogeochemical-oyster-filtration model predicts that the presence of oysters (*Crassostrea virginica*) can improve, or reduce,  
854 water quality depending upon oyster abundance and location. *Ecol. Model.*, 496, 110833,  
855 <https://doi.org/10.1016/j.ecolmodel.2024.110833>, 2024.
- 856 Gazeau, F., Quiblier, C., Jansen, J. M., Gattuso, J. P., Middelburg, J. J., and Heip, C. H.: Impact of elevated CO<sub>2</sub> on shellfish  
857 calcification. *Geophys. Res. Lett.*, 34, 7, <https://doi.org/10.1029/2006GL028554>, 2007.
- 858 Gobler, C. J. and Talmage, S. C.: Physiological response and resilience of early life-stage Eastern oysters (*Crassostrea  
859 virginica*) to past, present and future ocean acidification, *Conserv. Physiol.*, 2, cou004,  
860 <https://doi.org/10.1093/conphys/cou004>, 2014.
- 861 Gouletquer, P., Soletchnik, P., Le Moine, O., Razet, D., Geairon, P., and Faury, N.: Summer mortality of the Pacific cupped  
862 oyster *Crassostrea gigas* in the Bay of Marennes-Oléron (France), *CIEM Conseil International pour l'Exploration de la Mer*,  
863 1998.
- 864 Gmelin, J. F.: Caroli a Linnaei Systema Naturae per Regna Tria Naturae, *Systema Naturae, Linnaeus*, 13, 3021–3910, 1791.



- 865 Gruber, N., Clement, D., Carter, B. R., Feely, R. A., Heuven, S. van, Hoppema, M., Ishii, M., Key, R. M., Kozyr, A., Lauvset,  
866 S. K., Monaco, C. L., Mathis, J. T., Murata, A., Olsen, A., Perez, F. F., Sabine, C. L., Tanhua, T., and Wanninkhof, R.: The  
867 oceanic sink for anthropogenic CO<sub>2</sub> from 1994 to 2007, *Science*, 363, 1193–1199, <https://doi.org/10.1126/science.aau5153>,  
868 2019.
- 869 Guévelou, E., Carnegie, R. B., Small, J. M., Hudson, K., Reece, K. S., and Rybovich, M. M.: Tracking Triploid Mortalities  
870 of Eastern Oysters *Crassostrea virginica* in the Virginia Portion of the Chesapeake Bay, *J. Shellfish Res.*, 38, 101–113,  
871 <https://doi.org/10.2983/035.038.0110>, 2019.
- 872 Hasler, C. T., Jeffrey, J. D., Schneider, E. V. C., Hannan, K. D., Tix, J. A., and Suski, C. D.: Biological consequences of weak  
873 acidification caused by elevated carbon dioxide in freshwater ecosystems, *Hydrobiologia*, 806, 1–12,  
874 <https://doi.org/10.1007/s10750-017-3332-y>, 2018.
- 875 Herrmann, M., Najjar, R. G., Da, F., Friedman, J. R., Friedrichs, M. A. M., Goldberger, S., Menendez, A., Shadwick, E. H.,  
876 Stets, E. G., and St-Laurent, P.: Challenges in Quantifying Air-Water Carbon Dioxide Flux Using Estuarine Water Quality  
877 Data: Case Study for Chesapeake Bay, *J. Geophys. Res.: Oceans*, 125, e2019JC015610, <https://doi.org/10.1029/2019jc015610>,  
878 2020.
- 879 Hersbach, H., Bell, B., Berrisford, P., Hirahara, S., Horányi, A., Muñoz-Sabater, J., Nicolas, J., Peubey, C., Radu, R., Schepers,  
880 D., Simmons, A., Soci, C., Abdalla, S., Abellan, X., Balsamo, G., Bechtold, P., Biavati, G., Bidlot, J., Bonavita, M., Chiara,  
881 G., Dahlgren, P., Dee, D., Diamantakis, M., Dragani, R., Flemming, J., Forbes, R., Fuentes, M., Geer, A., Haimberger, L.,  
882 Healy, S., Hogan, R. J., Hólm, E., Janisková, M., Keeley, S., Laloyaux, P., Lopez, P., Lupu, C., Radnoti, G., Rosnay, P.,  
883 Rozum, I., Vamborg, F., Villaume, S., and Thépaut, J.: The ERA5 global reanalysis, *Q. J. R. Meteorol. Soc.*, 146, 1999–2049,  
884 <https://doi.org/10.1002/qj.3803>, 2020.
- 885 Hinson, K. E., Friedrichs, M. A. M., St-Laurent, P., Da, F., and Najjar, R. G.: Extent and Causes of Chesapeake Bay Warming,  
886 *JAWRA J. Am. Water Resour. Assoc.*, 58, 805–825, <https://doi.org/10.1111/1752-1688.12916>, 2022.
- 887 Hinson, K. E., Friedrichs, M. A. M., Najjar, R. G., Herrmann, M., Bian, Z., Bhatt, G., St-Laurent, P., Tian, H., and Shenk, G.:  
888 Impacts and uncertainties of climate-induced changes in watershed inputs on estuarine hypoxia, *Biogeosciences*, 20, 1937–  
889 1961, <https://doi.org/10.5194/bg-20-1937-2023>, 2023.
- 890 Himes, A.R., Schatz, A. and Rivest, E.B.: Differences in larval acidification tolerance among populations of the eastern oyster,  
891 *Crassostrea virginica*. *J. Exp. Mar. Biol. Ecol.*, 577, 152023, <https://doi.org/10.1016/j.jembe.2024.152023>, 2024.
- 892 Hochachka, P. W. and Somero, G. N.: *Biochemical Adaptation: Mechanism and Processing Physiological Evolution*. Oxford  
893 University Press, 2002.
- 894 Hofmann, G. E. and Hand, S. C.: Global arrest of translation during invertebrate quiescence., *Proc. Natl. Acad. Sci.*, 91, 8492–  
895 8496, <https://doi.org/10.1073/pnas.91.18.8492>, 1994.
- 896 Hopkinson, C. S., Buffam, I., Hobbie, J., Vallino, J., Perdue, M., Eversmeyer, B., Prahl, F., Covert, J., Hodson, R., Moran, M.  
897 A., Smith, E., Baross, J., Crump, B., Findlay, S., and Foreman, K.: Terrestrial inputs of organic matter to coastal ecosystems:



- 898 An intercomparison of chemical characteristics and bioavailability, *Biogeochemistry*, 43, 211–234,  
899 <https://doi.org/10.1023/a:1006016030299>, 1998.
- 900 Hudson, K.: Virginia Shellfish Aquaculture Situation and Outlook Report: Results of the 2018 Virginia Shellfish Aquaculture  
901 Crop Reporting Survey, 2019.
- 902 Intergovernmental Panel on Climate Change: IPCC Special Report on the Ocean and Cryosphere in a Changing Climate [H.-  
903 O. Pörtner, D.C. Roberts, V. Masson-Delmotte, P. Zhai, M. Tignor, E. Poloczanska, K. Mintenbeck, A. Alegría, M. Nicolai,  
904 A. Okem, J. Petzold, B. Rama, N.M. Weyer (eds.)]. Cambridge University Press, Cambridge, UK and New York, NY, USA,  
905 755 pp. <https://doi.org/10.1017/9781009157964>, 2019.
- 906 Intergovernmental Panel on Climate Change: The Physical Science Basis, 673–816,  
907 <https://doi.org/10.1017/9781009157896.007>, 2021.
- 908 Irby, I. D., Friedrichs, M. A. M., Friedrichs, C. T., Bever, A. J., Hood, R. R., Lanerolle, L. W. J., Li, M., Linker, L., Scully,  
909 M. E., Sellner, K., Shen, J., Testa, J., Wang, H., Wang, P., and Xia, M.: Challenges associated with modeling low-oxygen  
910 waters in Chesapeake Bay: a multiple model comparison, *Biogeosciences*, 13, 2011–2028, [https://doi.org/10.5194/bg-13-](https://doi.org/10.5194/bg-13-2011-2016)  
911 2011-2016, 2016.
- 912 Irby, I. D., Friedrichs, M. A. M., Da, F., and Hinson, K. E.: The competing impacts of climate change and nutrient reductions  
913 on dissolved oxygen in Chesapeake Bay, *Biogeosciences*, 15, 2649–2668, <https://doi.org/10.5194/bg-15-2649-2018>, 2018.
- 914 Jewett, L. and Romanou, A.: Ocean acidification and other ocean changes. In: *Climate Science Special Report: Fourth National  
915 Climate Assessment, Volume I* [Wuebbles, D.J., D.W. Fahey, K.A. Hibbard, D.J. Dokken, B.C. Stewart, and T.K. Maycock  
916 (eds.)]. U.S. Global Change Research Program, Washington, DC, USA, pp. 364–392, doi: 10.7930/J0QV3JQB, 2017.
- 917 Jones, H. R., Johnson, K. M., and Kelly, M. W.: Synergistic Effects of Temperature and Salinity on the Gene Expression and  
918 Physiology of *Crassostrea virginica*, *Integr. Comp. Biol.*, 59, 306–319, <https://doi.org/10.1093/icb/icz035>, 2019.
- 919 Jordan, S. J.: Sedimentation and remineralization associated with biodeposition by the American oyster *Crassostrea virginica*  
920 (Gmelin). University of Maryland, College Park, 1987.
- 921 Kellogg, M. L., Brush, M., and Cornwell, J. C.: An updated model for estimating the TMDL- related benefits of oyster reef  
922 restoration, A final report to The Nature Conservancy and Oyster Recovery Partnership, 2018.
- 923 Kelly, C. J., Laramore, S. E., Scarpa, J., and Newell, R. I. E.: Seasonal Comparison of Physiological Adaptation and Growth  
924 of Suminoe (*Crassostrea ariakensis*) and Eastern (*Crassostrea virginica*) Oysters, *J. Shellfish Res.*, 30, 737–749,  
925 <https://doi.org/10.2983/035.030.0314>, 2011.
- 926 Kemp, W., Boynton, W., Adolf, J., Boesch, D., Boicourt, W., Brush, G., Cornwell, J., Fisher, T., Glibert, P., Hagy, J., Harding,  
927 L., Houde, E., Kimmel, D., Miller, W., Newell, R., Roman, M., Smith, E., and Stevenson, J.: Eutrophication of Chesapeake  
928 Bay: historical trends and ecological interactions, *Mar. Ecol. Prog. Ser.*, 303, 1–29, <https://doi.org/10.3354/meps303001>, 2005.
- 929 Kingsley-Smith, P. R., Harwell, H. D., Kellogg, M. L., Allen, S. M., Allen, S. K., Meritt, D. W., Paynter, K. T., and  
930 Luckenbach, M. W.: Survival and Growth of Triploid *Crassostrea virginica* (Gmelin, 1791) and *C. ariakensis* (Fujita, 1913) in



- 931 Bottom Environments of Chesapeake Bay: Implications for an Introduction, *J. Shellfish Res.*, 28, 169–184,  
932 <https://doi.org/10.2983/035.028.0201>, 2009.
- 933 La Peyre, M.K., Eberline, B.S., Soniat, T.M. and La Peyre, J.F.: Differences in extreme low salinity timing and duration  
934 differentially affect eastern oyster (*Crassostrea virginica*) size class growth and mortality in Breton Sound, LA, *Estuar. Coast.*  
935 *Shelf Sci.*, 135, 146–157, 2013.
- 936 Lake, S. and Brush, M.: Modeling estuarine response to load reductions in a warmer climate: York River Estuary, Virginia,  
937 USA, *Mar. Ecol. Prog. Ser.*, 538, 81–98, <https://doi.org/10.3354/meps11448>, 2015.
- 938 Lavaud, R., Peyre, M. K. L., Justic, D., and Peyre, J. F. L.: Dynamic Energy Budget modelling to predict eastern oyster growth,  
939 reproduction, and mortality under river management and climate change scenarios, *Estuar., Coast. Shelf Sci.*, 251, 107188,  
940 <https://doi.org/10.1016/j.ecss.2021.107188>, 2021.
- 941 Lavaud, R., Peyre, M. K. L., Couvillion, B., Pollack, J. B., Brown, V., Palmer, T. A., and Keim, B.: Predicting restoration and  
942 aquaculture potential of eastern oysters through an eco-physiological mechanistic model, *Ecol. Model.*, 489, 110603,  
943 <https://doi.org/10.1016/j.ecolmodel.2023.110603>, 2024.
- 944 Lemasson, A. J., Hall-Spencer, J. M., Fletcher, S., Provstgaard-Morys, S., and Knights, A. M.: Indications of future  
945 performance of native and non-native adult oysters under acidification and warming, *Mar. Environ. Res.*, 142, 178–189,  
946 <https://doi.org/10.1016/j.marenvres.2018.10.003>, 2018.
- 947 Li, M., Lee, Y. J., Testa, J. M., Li, Y., Ni, W., Kemp, W. M., and Toro, D. M. D.: What drives interannual variability of  
948 hypoxia in Chesapeake Bay: Climate forcing versus nutrient loading?, *Geophys. Res. Lett.*, 43, 2127–2134,  
949 <https://doi.org/10.1002/2015gl067334>, 2016.
- 950 Liddel, M. K.: A von Bertalanffy based model for the estimation of oyster (*Crassostrea virginica*) growth on restored oyster  
951 reefs in Chesapeake Bay, 2008.
- 952 Liu, Z., Zhou, Z., Zhang, Y., Wang, L., Song, X., Wang, W., Zheng, Y., Zong, Y., Lv, Z., and Song, L.: Ocean acidification  
953 inhibits initial shell formation of oyster larvae by suppressing the biosynthesis of serotonin and dopamine. *Sci. Total Environ.*,  
954 735, 139469, <https://doi.org/10.1016/j.scitotenv.2020.139469>, 2020.
- 955 Loosanoff, V. L.: Some aspects of behavior of oysters at different temperatures, *Biol. Bull.*, 114, 57–70,  
956 <https://doi.org/10.2307/1538965>, 1958.
- 957 López-Urrutia, Á., Martin, E. S., Harris, R. P., and Irigoien, X.: Scaling the metabolic balance of the oceans, *Proc. Natl. Acad.*  
958 *Sci.*, 103, 8739–8744, <https://doi.org/10.1073/pnas.0601137103>, 2006.
- 959 Lowe, A. T., Kobelt, J., Horwith, M., and Ruesink, J.: Ability of Eelgrass to Alter Oyster Growth and Physiology Is Spatially  
960 Limited and Offset by Increasing Predation Risk, *Estuaries Coasts*, 42, 743–754, [https://doi.org/10.1007/s12237-018-00488-](https://doi.org/10.1007/s12237-018-00488-9)  
961 9, 2019.
- 962 Lutier, M., Di Poi, C., Gazeau, F., Appolis, A., Le Luyer, J., and Pernet, F.: Revisiting tolerance to ocean acidification: insights  
963 from a new framework combining physiological and molecular tipping points of Pacific oyster. *Glob. Change Bio.*, 28(10),  
964 3333–3348, <https://doi.org/10.1111/gcb.16101>, 2022.



- 965 Mazarrasa, I., Marbà, N., Lovelock, C. E., Serrano, O., Lavery, P. S., Fourqurean, J. W., Kennedy, H., Mateo, M. A., Krause-  
966 Jensen, D., Steven, A. D. L., and Duarte, C. M.: Seagrass meadows as a globally significant carbonate reservoir,  
967 *Biogeosciences*, 12, 4993–5003, <https://doi.org/10.5194/bg-12-4993-2015>, 2015.
- 968 Matoo, O. B., Lannig, G., Bock, C., and Sokolova, I. M.: Temperature but not ocean acidification affects energy metabolism  
969 and enzyme activities in the blue mussel, *Mytilus edulis*. *Ecol. Evol.*, 11(7), 3366–3379, <https://doi.org/10.1002/ece3.7289>,  
970 2021.
- 971 Medeiros, I. P. M., and Souza, M. M.: Acid times in physiology: a systematic review of the effects of ocean acidification on  
972 calcifying invertebrates. *Environmental Research*, 116019, <https://doi.org/10.1016/j.envres.2023.116019>, 2023
- 973 Melzner, F., Mark, F.C., Seibel, B.A. and Tomanek, L.: Ocean acidification and coastal marine invertebrates: tracking CO<sub>2</sub>  
974 effects from seawater to the cell. *Annu. Rev. Mar. Sci.*, 12, pp.499–523, <https://doi.org/10.1146/annurev-marine-010419->  
975 010658, 2020.
- 976 Mitchell, M., Herman, J., Bilkovic, D. M., and Hershner, C.: Marsh persistence under sea-level rise is controlled by multiple,  
977 geologically variable stressors, *Ecosyst. Heal. Sustain.*, 3, 1379888, <https://doi.org/10.1080/20964129.2017.1396009>, 2017.
- 978 Mizuta, D. D., Silveira, N., Fischer, C. E., and Lemos, D.: Interannual variation in commercial oyster (*Crassostrea gigas*)  
979 farming in the sea (Florianópolis, Brazil, 27°44' S; 48°33' W) in relation to temperature, chlorophyll a and associated  
980 oceanographic conditions, *Aquaculture*, 366, 105–114, <https://doi.org/10.1016/j.aquaculture.2012.09.011>, 2012.
- 981 Mizuta, D. D. and Wikfors, G. H.: Seeking the perfect oyster shell: a brief review of current knowledge, *Rev. Aquac.*, 11, 586–  
982 602, <https://doi.org/10.1111/raq.12247>, 2019.
- 983 Moore, K. A., Orth, R. J., and Wilcox, D. J.: Assessment of the Abundance of Submersed Aquatic Vegetation (SAV)  
984 Communities in the Chesapeake Bay and its Use in SAV Management, in: Remote Sensing and Geospatial Technologies for  
985 Coastal Ecosystem Assessment and Management, <https://doi.org/10.1007/978-3-540-88183-4>, 2009.
- 986 Moore-Maley, B. L., Allen, S. E., and Ianson, D.: Locally driven interannual variability of near-surface pH and  $\Omega_A$  in the  
987 Strait of Georgia, *J. Geophys. Res.: Oceans*, 121, 1600–1625, <https://doi.org/10.1002/2015jc011118>, 2016.
- 988 Moriarty, J. M., Friedrichs, M. A. M., and Harris, C. K.: Seabed Resuspension in the Chesapeake Bay: Implications for  
989 Biogeochemical Cycling and Hypoxia, *Estuaries Coasts*, 44, 103–122, <https://doi.org/10.1007/s12237-020-00763-8>, 2021.
- 990 Najjar, R. G., Herrmann, M., Valle, S. M. C. D., Friedman, J. R., Friedrichs, M. A. M., Harris, L. A., Shadwick, E. H., Stets,  
991 E. G., and Woodland, R. J.: Alkalinity in Tidal Tributaries of the Chesapeake Bay, *J. Geophys. Res.: Oceans*, 125,  
992 <https://doi.org/10.1029/2019jc015597>, 2020.
- 993 Newell, R. I. E. and Koch, E. W.: Modeling seagrass density and distribution in response to changes in turbidity stemming  
994 from bivalve filtration and seagrass sediment stabilization, *Estuaries*, 27, 793–806, <https://doi.org/10.1007/bf02912041>, 2004.
- 995 Ni, W., Li, M., and Testa, J. M.: Discerning effects of warming, sea level rise and nutrient management on long-term hypoxia  
996 trends in Chesapeake Bay, *Sci. Total Environ.*, 737, 139717, <https://doi.org/10.1016/j.scitotenv.2020.139717>, 2020.
- 997 Olson, M.: Guide to Using Chesapeake Bay Program Water Quality Monitoring Data, Chesapeake Bay Program, Annapolis,  
998 MD, 2012.





- 999 Nichols, M.M., Kim, S.C. and Brouwer, C.M.: Sediment Characterization of Chesapeake Bay and Its Tributaries, 1991.
- 1000 Orr, J.C., Fabry, V.J., Aumont, O., Bopp, L., Doney, S.C., Feely, R.A., Gnanadesikan, A., Gruber, N., Ishida, A., Joos, F. and  
1001 Key, R.M.: Anthropogenic ocean acidification over the twenty-first century and its impact on calcifying organisms,  
1002 Nature, 437, 681–686, <https://doi.org/10.1038/nature04095>, 2005.
- 1003 Orth, R. J., Nowak, J. F., Wilcox, D. J., Whiting, J. R., and Nagey, L. S.: Distribution of Submerged Aquatic Vegetation in the  
1004 Chesapeake Bay and Tributaries and the Coastal Bays, Am. Zoöl., 3, 315–317, <https://doi.org/10.1093/icb/3.3.315>, 1998.
- 1005 Pacella, S.R., Brown, C.A., Kaldy, J.E., Labiosa, R.G., Hales, B., Mochon Collura, T.C. and Waldbusser, G.G.: Quantifying  
1006 the combined impacts of anthropogenic CO<sub>2</sub> emissions and watershed alteration on estuary acidification at biologically-  
1007 relevant time scales: a case study from Tillamook Bay, OR, USA. Front. Mar. Sci., 11, 1293955,  
1008 <https://doi.org/10.3389/fmars.2024.1293955>, 2024.
- 1009 Palmer, S. C. J., Gernez, P. M., Thomas, Y., Simis, S., Miller, P. I., Glize, P., and Barillé, L.: Remote Sensing-Driven Pacific  
1010 Oyster (*Crassostrea gigas*) Growth Modeling to Inform Offshore Aquaculture Site Selection, Front. Mar. Sci., 6, 802,  
1011 <https://doi.org/10.3389/fmars.2019.00802>, 2020.
- 1012 Palmer, S. C. J., Barillé, L., Kay, S., Ciavatta, S., Buck, B., and Gernez, P.: Pacific oyster (*Crassostrea gigas*) growth modelling  
1013 and indicators for offshore aquaculture in Europe under climate change uncertainty, Aquaculture, 532, 736116,  
1014 <https://doi.org/10.1016/j.aquaculture.2020.736116>, 2021.
- 1015 Paynter, K. T., Goodwin, J. D., Chen, M. E., Ward, N. J., Sherman, M. W., Meritt, D. W., and Allen, S. K.: *Crassostrea*  
1016 *ariakensis* in Chesapeake Bay: Growth, Disease and Mortality in Shallow Subtidal Environments, J. Shellfish Res., 27, 509–  
1017 515, [https://doi.org/10.2983/0730-8000\(2008\)27\[509:caicbg\]2.0.co;2](https://doi.org/10.2983/0730-8000(2008)27[509:caicbg]2.0.co;2), 2008.
- 1018 Peyre, M. K. L., Eberline, B. S., Soniat, T. M., and Peyre, J. F. L.: Differences in extreme low salinity timing and duration  
1019 differentially affect eastern oyster (*Crassostrea virginica*) size class growth and mortality in Breton Sound, LA, Estuar., Coast.  
1020 Shelf Sci., 135, 146–157, <https://doi.org/10.1016/j.ecss.2013.10.001>, 2013.
- 1021 Planton, S., Déqué, M., Chauvin, F., and Terray, L.: Expected impacts of climate change on extreme climate events, C. R.  
1022 Geosci., 340, 564–574, <https://doi.org/10.1016/j.crte.2008.07.009>, 2008.
- 1023 Poach, M., Munroe, D., Vasslides, J., Abrahamsen, I. and Coffey, N.: Monitoring coastal acidification along the US East coast:  
1024 concerns for shellfish production. Bull. Jap. Fish. Res. Edu. Agen. No, 49, 53–64, 2019.
- 1025 Ramajo, L., Pérez-León, E., Hendriks, I. E., Marbà, N., Krause-Jensen, D., Sejr, M. K., Blicher, M. E., Lagos, N. A., Olsen,  
1026 Y. S., and Duarte, C. M.: Food supply confers calcifiers resistance to ocean acidification, Sci. Rep., 6, 19374,  
1027 <https://doi.org/10.1038/srep19374>, 2016.
- 1028 Raymond, P. A., Bauer, J. E., and Cole, J. J.: Atmospheric CO<sub>2</sub> evasion, dissolved inorganic carbon production, and net  
1029 heterotrophy in the York River estuary, Limnol. Oceanogr., 45, 1707–1717, <https://doi.org/10.4319/lo.2000.45.8.1707>, 2000.
- 1030 Riahi, K., Rao, S., Krey, V., Cho, C., Chirkov, V., Fischer, G., Kindermann, G., Nakicenovic, N., and Rafaj, P.: RCP 8.5—A  
1031 scenario of comparatively high greenhouse gas emissions, Clim. Chang., 109, 33, <https://doi.org/10.1007/s10584-011-0149->  
1032 y, 2011.



- 1033 Redfield, A.C.: On the proportions of organic derivatives in sea water and their relation to the composition of plankton,  
1034 University Press of Liverpool, Liverpool, UK, 1934.
- 1035 Reid, J.M., Reid, J.A., Jenkins, C.J., Hastings, M.E., Williams, S.J. and Poppe, L.J.: usSEABED: Atlantic coast offshore  
1036 surficial sediment data release, US Geological Survey Data Series, 118, 2005.
- 1037 Rivest, E.B., Brush, M., Zimmerman, R., Hill, V.,” Can Meadows of Submerged Aquatic Vegetation (SAV) Mitigate Ocean  
1038 Acidification Thresholds for Eastern Oysters in the Chesapeake Bay? Final report, NOAA Ocean Acidification Program.  
1039 Award number NA18NOS4780177, 2023.
- 1040 Roden, E. and Tuttle, J.: Inorganic sulfur cycling in mid and lower Chesapeake Bay sediments, *Mar. Ecol. Prog. Ser.*, 93, 101–  
1041 118, <https://doi.org/10.3354/meps093101>, 1993.
- 1042 Rybovich, M., Peyre, M. K. L., Hall, S. G., and Peyre, J. F. L.: Increased Temperatures Combined with Lowered Salinities  
1043 Differentially Impact Oyster Size Class Growth and Mortality, *J. Shellfish Res.*, 35, 101–113,  
1044 <https://doi.org/10.2983/035.035.0112>, 2016.
- 1045 Saavedra, L., Bastías, M., Mendoza, P., Lagos, N. A., García-Herrera, C., Ponce, V., Alvarez, F., and Llanos-Rivera, A.:  
1046 Environmental correlates of oyster farming in an upwelling system: Implication upon growth, biomass production, shell  
1047 strength and organic composition, *Mar. Environ. Res.*, <https://doi.org/10.1016/j.marenvres.2024.106489>, 2024.
- 1048 Salisbury, J., Green, M., Hunt, C., and Campbell, J.: Coastal Acidification by Rivers: A Threat to Shellfish?, *Eos, Trans. Am.*  
1049 *Geophys. Union*, 89, 513–513, <https://doi.org/10.1029/2008eo500001>, 2008.
- 1050 Schwaner, C., Barbosa, M., Schwemmer, T. G., Espinosa, E. P., and Allam, B.: Increased Food Resources Help Eastern Oyster  
1051 Mitigate the Negative Impacts of Coastal Acidification, *Animals*, 13, 1161, <https://doi.org/10.3390/ani13071161>, 2023.
- 1052 Simone, M. N., Schulz, K. G., Oakes, J. M., and Eyre, B. D.: Warming and ocean acidification may decrease estuarine  
1053 dissolved organic carbon export to the ocean, *Biogeosciences*, 18, 1823–1838, <https://doi.org/10.5194/bg-18-1823-2021>, 2021.
- 1054 Nixon, S.W.: Coastal marine eutrophication: A definition, social causes, and future concerns, *Ophelia*, 41, 199–219,  
1055 <https://doi.org/10.1080/00785236.1995.10422044>, 1995.
- 1056 Shadwick, E. H., Friedrichs, M. A. M., Najjar, R. G., Meo, O. A. D., Friedman, J. R., Da, F., and Reay, W. G.: High-Frequency  
1057 CO<sub>2</sub> System Variability Over the Winter-to-Spring Transition in a Coastal Plain Estuary, *J. Geophys. Res.: Oceans*, 124, 7626–  
1058 7642, <https://doi.org/10.1029/2019jc015246>, 2019.
- 1059 Shchepetkin, A. F. and McWilliams, J. C.: The regional oceanic modeling system (ROMS): a split-explicit, free-surface,  
1060 topography-following-coordinate oceanic model, *Ocean Model.*, 9, 347–404, <https://doi.org/10.1016/j.ocemod.2004.08.002>,  
1061 2005.
- 1062 Shen, C., Testa, J. M., Li, M., Cai, W., Waldbusser, G. G., Ni, W., Kemp, W. M., Cornwell, J., Chen, B., Brodeur, J., and Su,  
1063 J.: Controls on Carbonate System Dynamics in a Coastal Plain Estuary: A Modeling Study, *J. Geophys. Res.: Biogeosciences*,  
1064 124, 61–78, <https://doi.org/10.1029/2018jg004802>, 2019a.



- 1065 Shen, C., Testa, J. M., Ni, W., Cai, W., Li, M., and Kemp, W. M.: Ecosystem Metabolism and Carbon Balance in Chesapeake  
1066 Bay: A 30-Year Analysis Using a Coupled Hydrodynamic-Biogeochemical Model, *J. Geophys. Res.: Oceans*, 124, 6141–  
1067 6153, <https://doi.org/10.1029/2019jc015296>, 2019b.
- 1068 Shen, C., Testa, J. M., Li, M., and Cai, W.: Understanding Anthropogenic Impacts on pH and Aragonite Saturation State in  
1069 Chesapeake Bay: Insights From a 30-Year Model Study, *J. Geophys. Res.: Biogeosciences*, 125,  
1070 <https://doi.org/10.1029/2019jg005620>, 2020.
- 1071 Siedlecki, S. A., Pilcher, D., Howard, E. M., Deutsch, C., MacCready, P., Norton, E. L., Frenzel, H., Newton, J., Feely, R. A.,  
1072 Alin, S. R., and Klinger, T.: Coastal processes modify projections of some climate-driven stressors in the California Current  
1073 System, *Biogeosciences*, 18, 2871–2890, <https://doi.org/10.5194/bg-18-2871-2021>, 2021a.
- 1074 Siedlecki, S., Salisbury, J., Gledhill, D., Bastidas, C., Meseck, S., McGarry, K., Hunt, C., Alexander, M., Lavoie, D., Wang,  
1075 Z., Scott, J., Brady, D., Mlsna, I., Azetsu-Scott, K., Liberti, C., Melrose, D., White, M., Pershing, A., Vandemark, D.,  
1076 Townsend, D., Chen, C., Mook, W., and Morrison, R.: Projecting ocean acidification impacts for the Gulf of Maine to 2050,  
1077 *Elem.: Sci. Anthr.*, 9, <https://doi.org/10.1525/elementa.2020.00062>, 2021b.
- 1078 Speights, C. J., Silliman, B. R., and McCoy, M. W.: The effects of elevated temperature and dissolved  $p\text{CO}_2$  on a marine  
1079 foundation species, *Ecol. Evol.*, 7, 3808–3814, <https://doi.org/10.1002/ece3.2969>, 2017.
- 1080 Simpson, E., Ianson, D., Kohfeld, K. E., Franco, A. C., Covert, P. A., Davelaar, M., and Perreault, Y.: Variability and drivers  
1081 of carbonate chemistry at shellfish aquaculture sites in the Salish Sea, British Columbia. *Biogeosciences*, 21, 1323-1353,  
1082 <https://doi.org/10.5194/bg-21-1323-2024>, 2024.
- 1083 Stevens, A. and Gobler, C.: Interactive effects of acidification, hypoxia, and thermal stress on growth, respiration, and survival  
1084 of four North Atlantic bivalves, *Mar. Ecol. Prog. Ser.*, 604, 143–161, <https://doi.org/10.3354/meps12725>, 2018.
- 1085 St-Laurent, P. and Friedrichs, M. A. M.: On the Sensitivity of Coastal Hypoxia to Its External Physical Forcings, *J. Adv.*  
1086 *Model. Earth Syst.*, 16, <https://doi.org/10.1029/2023ms003845>, 2024.
- 1087 St-Laurent, P., Friedrichs, M. A. M., Najjar, R. G., Shadwick, E. H., Tian, H., and Yao, Y.: Relative impacts of global changes  
1088 and regional watershed changes on the inorganic carbon balance of the Chesapeake Bay, *Biogeosciences*, 17, 3779–3796,  
1089 <https://doi.org/10.5194/bg-17-3779-2020>, 2020.
- 1090 Su, J., Cai, W.-J., Brodeur, J., Chen, B., Hussain, N., Yao, Y., Ni, C., Testa, J. M., Li, M., Xie, X., Ni, W., Scaboo, K. M., Xu,  
1091 Y., Cornwell, J., Gurbisz, C., Owens, M. S., Waldbusser, G. G., Dai, M., and Kemp, W. M.: Chesapeake Bay acidification  
1092 buffered by spatially decoupled carbonate mineral cycling, *Nat. Geosci.*, 13, 441–447, [https://doi.org/10.1038/s41561-020-](https://doi.org/10.1038/s41561-020-0584-3)  
1093 0584-3, 2020.
- 1094 Swam, L. M., Couvillion, B., Callam, B., Peyre, J. F. L., and Peyre, M. K. L.: Defining oyster resource zones across coastal  
1095 Louisiana for restoration and aquaculture, *Ocean Coast. Manag.*, 225, 106178,  
1096 <https://doi.org/10.1016/j.ocecoaman.2022.106178>, 2022.



- 1097 Talmage, S. C. and Gobler, C. J.: Effects of Elevated Temperature and Carbon Dioxide on the Growth and Survival of Larvae  
1098 and Juveniles of Three Species of Northwest Atlantic Bivalves, PLoS ONE, 6, e26941,  
1099 <https://doi.org/10.1371/journal.pone.0026941>, 2011.
- 1100 Tian, R., Cerco, C. F., Bhatt, G., Linker, L. C., and Shenk, G. W.: Mechanisms Controlling Climate Warming Impact on the  
1101 Occurrence of Hypoxia in Chesapeake Bay, JAWRA J. Am. Water Resour. Assoc., 58, 855–875, <https://doi.org/10.1111/1752-1688.12907>, 2022.
- 1103 Thomsen, J., Haynert, K., Wegner, K. M., and Melzner, F.: Impact of seawater carbonate chemistry on the calcification of  
1104 marine bivalves, Biogeosciences, 12, 4209–4220, <https://doi.org/10.5194/bg-12-4209-2015>, 2015.
- 1105 Turner, J. S., St-Laurent, P., Friedrichs, M. A. M., and Friedrichs, C. T.: Effects of reduced shoreline erosion on Chesapeake  
1106 Bay water clarity, Sci. Total Environ., 769, 145157, <https://doi.org/10.1016/j.scitotenv.2021.145157>, 2021.
- 1107 van Heuven, S., D. Pierrot, J.W.B. Lewis, R.E., and Wallace, D.W.R.: MATLAB Program Developed for CO<sub>2</sub> System  
1108 Calculations. ORNL/CDIAC-105b. Carbon Dioxide Information Analysis Center, Oak Ridge National Laboratory, U.S.  
1109 Department of Energy, Oak Ridge, Tennessee. [https://doi.org/10.3334/CDIAC/otg.CO2SYS\\_MATLAB\\_v1.1](https://doi.org/10.3334/CDIAC/otg.CO2SYS_MATLAB_v1.1), 2011.
- 1110 VOSARA: <https://cmap22.vims.edu/VOSARA/>, last access: 28 January 2024.
- 1111 Waldbusser, G. G., Voigt, E. P., Bergschneider, H., Green, M. A., and Newell, R. I. E.: Biocalcification in the Eastern Oyster  
1112 (*Crassostrea virginica*) in Relation to Long-term Trends in Chesapeake Bay pH, Estuaries Coasts, 34, 221–231,  
1113 <https://doi.org/10.1007/s12237-010-9307-0>, 2011.
- 1114 Wallace, R. B., Baumann, H., Grear, J. S., Aller, R. C., and Gobler, C. J.: Coastal ocean acidification: The other eutrophication  
1115 problem, Estuar., Coast. Shelf Sci., 148, 1–13, <https://doi.org/10.1016/j.ecss.2014.05.027>, 2014.
- 1116 Warner, J. C., Defne, Z., Haas, K., and Arango, H. G.: A wetting and drying scheme for ROMS, Comput. Geosci., 58, 54–61,  
1117 <https://doi.org/10.1016/j.cageo.2013.05.004>, 2013.
- 1118 Zhang, Q., Fisher, T. R., Trentacoste, E. M., Buchanan, C., Gustafson, A. B., Karrh, R., Murphy, R. R., Keisman, J., Wu, C.,  
1119 Tian, R., Testa, J. M., and Tango, P. J.: Nutrient limitation of phytoplankton in Chesapeake Bay: Development of an empirical  
1120 approach for water-quality management, Water Res., 188, 116407, <https://doi.org/10.1016/j.watres.2020.116407>, 2021.